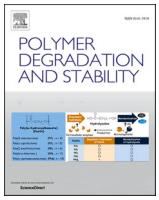
Polymer Degradation and Stability 234 (2025) 111257



Contents lists available at ScienceDirect

Polymer Degradation and Stability

journal homepage: www.journals.elsevier.com/polymer-degradation-and-stability





# New high UV transparency PV encapsulants: Properties and degradation after accelerated UV aging tests

Valeria Fiandra *, Lucio Sannino, Concetta Andreozzi, Giovanni Flaminio, Antonio Romano, Gabriella Rametta

*ENEA - Italian National Agency for New Technologies, Energy and Sustainable Economic Development, P.le E. Fermi 1, 80055, Portici, Naples, Italy*

ARTICLE INFO

*Keywords:*
High transparency PV encapsulants
UV aging
Polymer photo-degradation
Thermoplastic polyolefin
Polyolefin elastomer
Photovoltaic module

ABSTRACT

To increase the PV modules efficiency, it is very important to improve not only the solar cell production technology, but also the other materials needed in their manufacture. Encapsulant materials, used to ensure the long-term lifespan and stability of solar cells, play an important role in PV module reliability. In fact, most modules breakdowns are linked precisely to the type of polymeric film used in their manufacturing. A detailed understanding of the causes and processes of PV module degradation and material is crucial for a successful development of new components and design of durable and reliable PV module. This article focuses on new high UV transparency polymeric materials usable for Si-based cells encapsulation and carries out thorough testing to evaluate their damaging caused by exposure to UV radiation. To obtain a reasonable evaluation of reliability of these highly UV transparent films, they were exposed to accelerated aging in a climatic chamber and then the changes in their optical, chemical and structural properties were analysed. The evaluating of the effect of UV radiation was also carried out on electrical performance of PV mini-devices made in the laboratory with the new encapsulants. Results have shown that, between the different UV transparent films tested, thermoplastic polyolefin-based encapsulants have a higher stability in long-term behaviour.

## 1. Introduction

The encapsulant is a thin, transparent polymeric layer that is applied to the top and bottom of the solar cells, to protect them from environmental damage and improve their mechanical stability. EVA has been for several decades and is still the most commonly used encapsulant in solar panels manufacturing because it meets some important requirements. It is a highly transparent material and resistant to UV radiation, offers excellent adhesion to glass and solar cells and has a low water vapor transmission rate [1]. However, in order to enhance durability and reliability of PV modules and overcome some critical issues related to the use of EVA, in recent years, research has been directed towards the formulation of new encapsulants. In this perspective, for example, materials have been formulated that do not develop acetic acid during degradation, that have an improved UV cut-off below 350 nm, that require a lamination process with more favorable conditions in terms of reduced polymerization times and lower temperatures and pressures. Among these, new materials such as silicones, ionomers and polyolefins (PO) based encapsulants have been developed, which show greater chemical stability compared to EVA, less discoloration and opacity in operating conditions [2]. In particular, the new PO-based encapsulants have gained approval. They are thermally more stable than EVA and do not produce acetic acid due to chemical degradation induced by different types of stress during field operation of a PV module. Their thermal and chemical characteristics promise to maintain high performance of the module over time, extending its life and overcoming reliability problems related to EVA degradation. Some of these materials also have other interesting properties for photovoltaic applications, such as high transmittance, higher resistance to moisture and temperature changes and dielectric properties that allow to prevent or reduce the potential induced degradation (PID) effect [3,4].

EVA is a thermosetting film, while PO-based encapsulants can be of two types: thermosetting and thermoplastic. Thermosetting POs (POE) require a curing process like EVA and are mainly used for the encapsulation of conventional PV modules in crystalline silicon. During the lamination process, to achieve thermal and thermomechanical stability,

* Corresponding author at: DIN Laboratory, TERIN Department, ENEA - Italian National Agency for New Technologies, Energy and Sustainable Economic Development, Portici 80055 Naples, Italy.
*E-mail address:* valeria.fiandra@enea.it (V. Fiandra).

https://doi.org/10.1016/j.polymdegradstab.2025.111257
Received 3 October 2024; Received in revised form 23 January 2025; Accepted 7 February 2025
Available online 7 February 2025
0141-3910/© 2025 The Author(s). Published by Elsevier Ltd. This is an open access article under the CC BY license (http://creativecommons.org/licenses/by/4.0/).

hardening agents are added to the encapsulant so that chemical cross-linking occurs. However, this leaves reactive peroxides in the PV module, which can influence or accelerate degradation processes of the encapsulant itself and corrosion of the module. Thermoplastic PO (TPO) films melt during the module manufacturing process without forming chemical bonds between the polymer chains (cross-linking), do not contain peroxides, are recyclable and are mainly suitable for thin film modules. Therefore, in the PV module manufacturing, the properties of the encapsulant influence the lamination process, determining its reliability and durability. Baiamonte et al. have demonstrated that the lamination process of POE films leads to the formation of sheets with good rigidity and ductility and more stable than EVA, in terms of photo- and thermo-oxidation [5].

To date, in single glass modules, the front surface of the cells is encapsulated with a high transmittance EVA film, while the rear surface with a UV-cut EVA film. Instead, the use of POs is spreading in the manufacture of double glass and thin film modules. In particular, in double glass modules, a high transmittance POE film is used for both the front and rear parts of the cells, while thin film modules use UV-cut POE films and TPO films as the primary encapsulants [6,7].

The chemical and thermal characteristics of some POEs and TPOs make these materials more environmentally friendly materials than EVA because, could help maintain better performance of PV modules. In fact, more thermally stable encapsulants allow for more efficient energy conversion and could contribute to the longevity of the system. Furthermore, maintaining a high performance of a module over time allows for a more productive and sustainable investment in the long term and less waste production. On the other hand, the thermal and chemical characteristics of EVA cause defects and reliability issues in the module performance, sometimes leading to a premature end of their life and consequently generating an increase in waste. With a view to creating devices that fall within a circular economy, the use of polyolefin-based encapsulants could improve the life cycle of the module. In fact, to respond to the circular economy strategies of photovoltaics, it is necessary to reduce waste and among the materials that could be recovered from end-of-life modules, some PO-based encapsulants are recyclable materials, unlike EVA which cannot be recycled because it undergoes cross-linking during lamination [8]. Although several studies in the literature have been done on these new PO-based polymer materials, to date, very few works concern tests on modules made with POE and TPO to demonstrate their real durability and the effect of UV radiation on their electrical performance. Among them, Oreski et al. have made test modules with EVA, POE and TPO and have studied the long-term behaviour of these encapsulants by exposing the test modules to different combinations of stress factors: temperature, relative humidity and irradiation, in accelerated aging tests. After 3000 h of damp heat (DH) test, only the test module with EVA showed slight corrosion effects, while the UV aging test, conducted up to 2000 h of irradiation and 120 kWh/m$^2$ UV dose, did not cause any significant power loss for any of the three test modules [9]. Probably, increasing the stress induced on these materials is necessary to obtain more significant evidence about the effects of UV-induced degradation. In this work, UV aging tests, conducted on mini-PV devices made of EVA, POE and TPO, were pushed up to 6000 h of irradiation and 1800 kWh/m$^2$ UV dose, to highlight the degradation of all the different materials and verify how and how much it affects the loss of electrical performances of the mini-devices. The choice of the encapsulation material is very important for the performance of the modules. They work outdoors, are exposed to sunlight, rain, ice, snow, sand, for a long time. Since it is necessary to guarantee a lifetime of at least 25 years, it is necessary to constantly improve their production technology, also in terms of optical, chemical and mechanical characteristics of the encapsulants and efficiency of adhesion between materials, in order to guarantee optimal performance and reliability of the modules [10]. The decrease in module power is closely connected with the aging of the encapsulant materials and with PID effect [11]. In the case of a module made with EVA, the entry of water vapor in the structure causes the hydrolysis of the acetate group and acetic acid is produced. This reacts with the alkali precipitated on the surface of the glass and mobile Na ions are produced which, under the action of an external electric field, move on the surface of the cell. Instead, POs do not only present higher volumetric resistivities then EVA, but also lower permeability to moisture, thus preventing degradation due to PID caused by high voltages and moisture and maintaining good performance of the modules [12,13]. Since photovoltaic modules are subject to an occasional hot-spot temperature increase, films made of EVA and PO blends have also been tested to improve the thermal resistance to high temperature. In fact, it has been demonstrated that the presence of PO in small amounts increases the thermal resistance compared to pure EVA. In particular, encapsulating films made from EVA/POE blends, additivated with cross-linking and stabilizing agents, although they have slightly decreased breakage properties compared to neat EVA, show higher thermal resistance. These blends are considered good candidates as encapsulants alternative to EVA, for bifacial PV modules, also because show a transparency similar to that of neat EVA. However, they have a lower resistance to photoaging [14]. As well as having a high barrier performance for oxygen and moisture and a high dielectric constant to reduce PID, a good encapsulant should have an excellent chemical inertness, and an excellent resistance to UV radiation and thermal oxidation to avoid degradation [15]. In addition, the discoloration and embrittlement of the polymer materials, caused by exposure to UV light, make PV modules less durable over time [16,17]. Nowadays, in order to prevent the aging and degradation of cells and polymers, the encapsulant is designed to block UV rays of sunlight reaching PV cells. In detail, UV absorbing agents are added in their formulation, so that the UV stability of encapsulant films is remarkably improved [18]. However, the flip side of a so formulated encapsulant is that lesser light reach cells resulting in lesser module power generation. Moreover, even during cloudy and foggy weather, a high amount of UV rays is present in sun light, and on one hand this prevents a sharp drop in power generation even when ambient visible light is poor, on the other hand causes materials degradation. In recent years, technological advancement in the encapsulant formulation has led to more efficient PV modules in power generation. In fact, UV transparent and at the same time more UV resistant encapsulants have been formulated, which have helped improve the performance of the modules. A high UV transparency encapsulant is a material that does not contain any chromophore absorbing in the UV domain. The need to use highly UV transparent encapsulants was born, so that sunlight can pass through the entire wavelength range to maximize solar energy conversion efficiency [19]. Hence, in the manufacturing project of a PV module, the use or not of a UV transparent and UV resistant encapsulant is of particular importance. Manufacturers are paying more and more attention to the specific formulation of the encapsulant to obtain a material with high UV transparency and ensure that the module generates more power than standard encapsulants, throughout the year [20]. Currently, the challenge is to enhance the positive effects of the solar radiation, to improve PV modules performance, and to minimize the negative ones of encapsulant premature aging, so that the solar panels last longer [21].

This work focuses on a specific type of POs-based polymeric films encapsulants namely those with high UV transparency, investigating the optical characteristics, their chemical degradation and morphological and structural changes upon accelerated UV aging. We conduct a detailed study to specifically evaluate high UV transparency PV encapsulants in terms of performance and reliability and quantify the performance gain of the module made with this type of new PO-based film compared to that made with standard EVA. Furthermore, the operational stability of a PV module stressed with UV radiation has not yet been studied in relation to reliability of these specific new UV transparent encapsulant materials. Therefore, we investigate the durability and electrical performance of mini-devices made with this type of PO-based encapsulants, after accelerated aging, pushed up to a UV dose of 1800 kWh/m$^2$, in order to highlight significant signs of degradation in

**Table 1**
Commercial name and encapsulant films specifications.

| Sample | Thickness (μm) | Density (g/cm$^3$) | Lamination Conditions | Optical transmittance* (%) | UV-cut off wavelength (nm) | Melting temperature (°C) | Refractive index |
|---|---|---|---|---|---|---|---|
| EVA-05HTL | 450–500 | 0.92 | 10 min, 145–150 °C | 91 | 300 | 65–70 | 1.48 |
| POE-8110 | 450–800 | 0.88 | 4–11 min, 160 °C | 91 | 310 | 60–80 | 1.49 |
| TPO | 200–600 | 0.95 | 8–15 min, 140–160 °C | >91 | 355 | >90 | 1.48 |

* Values for laminated films.

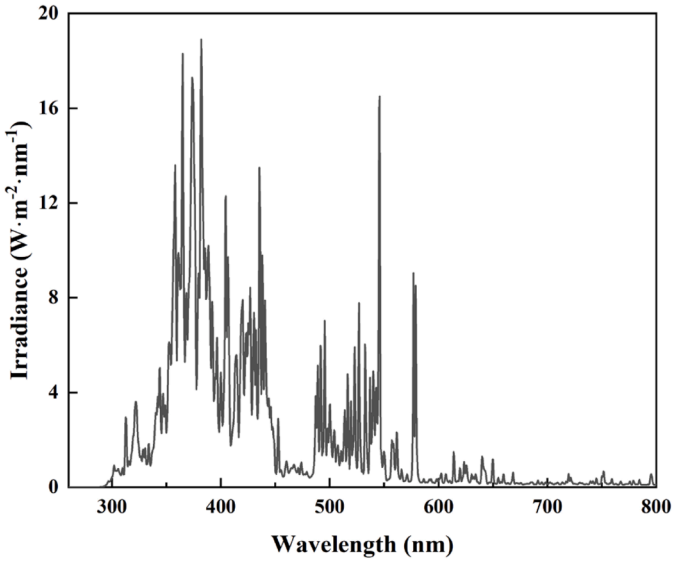



**Fig. 1.** Spectral irradiance distribution of 4 metal-halide arc lamps in the climatic chamber.

their electrical performance. In this way, this work contributes to provide useful and important information for the critical selection of reliable encapsulation materials for module design.

## 2. Materials and methods

### 2.1. Encapsulant films

Three different types of encapsulants were purchased from companies that produce polymer films for the photovoltaic sector. In detail, EVA-05HTL, POE-8110 and TPO were provided respectively by SATINAL, 3M and MG Lavorazioni Materie Plastiche. Table 1 shows the specifications of the films taken from the technical data sheets provided by the companies.

### 2.2. Encapsulant films lamination

Each polymeric film was laminated according to the indications provided in the respective technical data sheets, to simulate the manufacturing conditions of the module. A RISE Technology - CORE 1 laminator, equipped with an integrated controller for managing thermal cycles, a pressure cycle control system and a TAEVEO TECH MINI water chiller, was used for the samples lamination.

The laminating recipes for the three films differ in the maximum temperature and the dwell time at the given temperature. The laminator was preheated to 50 °C, afterwards, each sample was placed inside the laminator. In the initial step, the sample is heated to 80 °C, under vacuum, for 6 min, to allow the gases to escape. Then, through programmed heating, the laminating temperature is reached and the pressure is increased to 1 bar, to promote further elimination of gases. Once the set laminating time has elapsed, the system is cooled to room temperature. Maximum temperature e dwell time used for the samples are 150 °C and 700 s for EVA-05HTL, 160 °C and 900 s for POE-8110, 160 °C and 480 s for TPO.

### 2.3. Encapsulant films characterization

The optical properties of the encapsulants were measured by a Lambda 1050+ UV/Vis/NIR spectrometer (PerkinElmer). Spectra were recorded from 250 to 1250 nm, with a resolution of 1 nm and 8 scans, with an integrating sphere from 150 mm InGaAs. The samples were measured in transmittance mode.

Yellowness index (YI) measurements were carried out by a portable colorimeter (PCE Instruments, model: PCM-CSM 5), at 10° observer angle, 8°/d sphere geometry and a D65 light source. The white and black calibration has been made before the YI measurement and each sample has been measured in triplicate.

ATR-FTIR spectra were obtained by using a Spectrum Two Universal ATR Diamond—Perkin Elmer spectrometer, with a DTGS MIR detector, in attenuated total reflection (ATR) mode and were recorded in the range from 4000 to 400 cm$^{-1}$, with 32 scans and a spectral resolution of 4 cm$^{-1}$.

Each sample was directly placed on the UATR top plate mounted in the sample beam of the spectrometer, the measurements were taken by pressing each sample against the diamond crystal and measuring the absorption of the wave. All spectra were normalized with respect to the intensity of the peak at 2850 cm$^{-1}$, referred to methylene groups of polyethylene chain.

Raman spectra were carried out using a Renishaw inVia Reflex Raman spectrometer. The 514.5 nm frequency of a continuous wave diode-pumped solid state (DPSS) laser with an excitation power of 25 mW was used as the excitation source. The measurements were recorded in a spectral range from 100–4000 cm$^{-1}$ with 10 s of integration time and 50× magnification.

X-ray diffraction analysis was performed by using a Smartlab—Rigaku X Ray diffractometer working with Cu-$K_\alpha$ radiation ($\lambda$ = 1.54059 nm). The accelerating voltage and electric current were 40 kV and 40 mA, respectively. The samples were scanned in the range from 10° to 30° (2θ), with a scan speed of 1.2°/min.

The scanning electron microscopy (SEM) analyses were performed by using a Thermo Fisher Scientific Phenom ProX microscope, with an electron beam accelerated at 15 kV, equipped with a long-lifetime thermionic source of cerium hexaboride and a backscattered electron detector (BSD). The operational voltage range is set between 5 kV and 15 kV. The images were captured at an optimal voltage of 15 kV and at a resolution of 350x. The inset images were acquired at a resolution of 4900x. An EDX detector alongside the SEM was used to analyse the sample composition. A metal coating process was needed to make the samples conductive and improve the topographic contrast by providing secondary electrons. In particular, the samples were coated with a few nanometers of gold to reduce charging effects.

### 2.4. UV accelerated aging test on encapsulant films

UV accelerated weathering tests were carried out using a climatic

**Table 2**
%T at 550 nm and thickness of unaged encapsulants, before lamination (b.l.) and after lamination (a.l.).

| Unaged encapsulant | | Thickness | | % T at 550 nm |
|---|---|---|---|---|
| | | (μm) | RSD% | (400–800 nm) |
| EVA-05HTL | b.l. | 501 | 1.3 | 90 |
| | a.l. | 459 | 2.9 | 91 |
| POE-8110 | b.l. | 820 | 0.5 | 90 |
| | a.l. | 546 | 1.6 | 92 |
| TPO | b.l. | 468 | 0.9 | 90 |
| | a.l. | 458 | 0.5 | 90 |

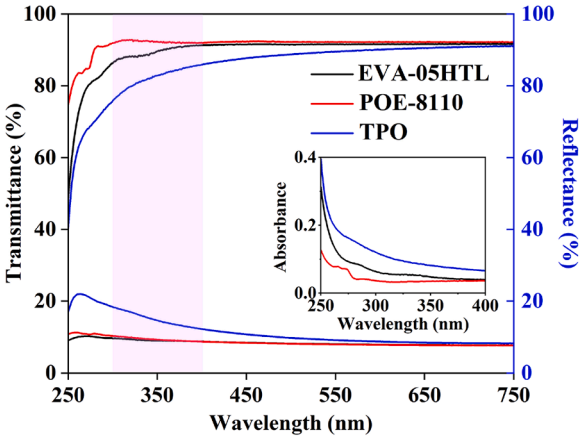



**Fig. 2.** UV–vis spectra of unaged EVA-05HTL, POE-8110 and TPO encapsulants, in transmittance and reflectance modes.

chamber type UV 3000 from Angelantoni Industries Spa (Italy), equipped with 4 metal-halide arc lamps type Ultramed 2000W OSRAM, to simulate the sunlight. Integrated into the chamber ceiling, 4 special filters, separated from the radiation unit, are installed to cut UVC radiation <280 nm. The radiation source is installed into the lamp house, which contains the parabolic segment reflector system. The reflectors are made out of anodised aluminium. A spectroradiometer type SR9910 V7 from Macam Photometrics Ltd (Scotland) was used to measure the lamp spectrum, recording the lamp intensity as a function of wavelength (240–800 nm), scan time of 100 ms per step and a step wavelength of 1 nm. To evaluate the UV dose to which the samples were exposed, the spectral irradiance of the lamps was measured. Fig. 1 shows the spectral irradiance distribution of the lamps in the climatic chamber. The fraction of radiant power relating to UV radiation in the wavelength range 300–400 nm was considered and is equal to 0.309 kW/m$^2$.

The aging test were carried out setting the temperature at 60 °C and relative humidity at 60 %. The three encapsulant films were aged in four consecutive steps corresponding to UV doses of 22, 74, 126 and 214 kWh/m$^2$.

### 2.5. Manufacture, UV accelerated aging and electrical measurements of PV mini-devices

Prototypes of PV mini-devices were manufactured in laboratory in order to evaluate the variation of their electrical characteristics during aging, depending on the encapsulant with which they were built. They were manufactured using half-cut cells, glass on the front, PET film on the back side and the three different polymers as encapsulants. Each prototype, with dimensions of 30 × 30 cm, was made by placing a half-cut cell between two fresh encapsulant layers, PET film on the back side of the encapsulant and the glass plate on the front side. Each prototype was laminated according to the recipe used for the encapsulant with which it was manufactured. However, the lamination recipe was slightly varied to take into account the heat transport resistance due to the overlapping material layers. To obtain uniform temperature distribution and repeatable lamination conditions, the temperature of the lamination plate was increased using a PLC controller, so that the average temperature between the lamination plate and that estimated by the thermocouple placed on the layer farthest from the heating plate was the one predicted by the recipe. The lamination time prescribed in the recipe for each polymer was instead respected.

The UV light accelerated weathering tests on the mini-devices were carried out in the same climate chamber used for the films, at the temperature of 60 °C and under 60 % relative humidity. Since the films encapsulated in PV mini-devices degrade much more slowly than standalone films, they require a higher UV dose to show signs of aging. To this purpose, the mini-devices have been exposed at the doses of 0, 22, 74, 126, 214, 600, 1200 and 1800 kWh/m$^2$.

The electrical characterization of the PV mini-devices was carried by a pulsed solar simulator PASAN IIIb, with a nominal sweep time of 10 ms, total irradiance of 1000 W/m$^2$, temperature of 25.0 ± 0.1 °C and corrected to Standard Test Condition STC (total irradiance of 1000 W/m$^2$, spectral irradiance of AM1.5g and cell temperature of 25 °C). Current-voltage (I–V) curve measurements were performed according to the CEI EN 61215-1 standard, before and after the UV aging tests. The mini-device, put on a holder, was electrically connected to the electronic load and the measurement was carried out during a single flash of 10 ms, keeping the temperature of the mini-device at 25 °C. To construct the I–V curve, 35–40 individual points were taken and each point was obtained by applying a constant voltage to the mini-device which was then subjected to a flash from the solar simulator at the desired irradiance level. Short-circuit current ($I_{SC}$), efficiency (Eff.), fill factor (FF) and power at maximum power point ($P_{MPP}$) were calculated from the measured I–V curves after each step of UV aging.

## 3. Results and discussions

### 3.1. Optical properties

The encapsulant in contact with the front surface of the solar cell in single glass PV modules or with both sides of the cell in double glass PV modules, should provide an optical transmittance of at least 90 % at wavelengths longer than 400 nm [22]. Table 2 lists the % transmittance values at 550 nm for the three unaged encapsulants, analysed before and after lamination. The choice of the wavelength at 550 nm allows to determine the maximum transmittance value of each film in the UV–vis spectral range and compare it with its changes during the aging [23,24]. After the lamination process, T% at 550 nm slightly increases only for EVA and POE. In particular, the small increase in transmittance for EVA is probably due to the low vinyl acetate content in the copolymer [25]. Thanks to their high transmittance, all three samples can be used such as single-layered and double-layered laminates.

Usually, in the range of wavelengths between 300 nm and 400 nm, most of the encapsulant films have a UV cut-off wavelength below which the transmittance is less than 10 %, due to the presence of UV absorbers added in the formulation [26]. Instead, these samples can efficiently transmit the light from the UV region to the entire visible spectrum. High transparency encapsulants are used to give a gain in power output of the PV module when compared to conventional EVA encapsulants. In fact, moving the UV cut-off of the encapsulants below 350 nm means increasing the spectral response of the solar cells in the blue/UV light spectrum, resulting in a relative power increase of more than 1 % [27]. Fig. 2 shows that in the UV region (250–400 nm) of the initial transmission spectrum, POE-8110 and EVA-05HTL have the highest transmittance compared to TPO.

The high UV transparency of these encapsulants compared to that of the traditional, is due to the reduced amount of UV stabilizing additives loaded in their formulations, to absorb and block the UV light. The light stabilizer and antioxidant additives show absorption at $\lambda < 280$ nm [28].

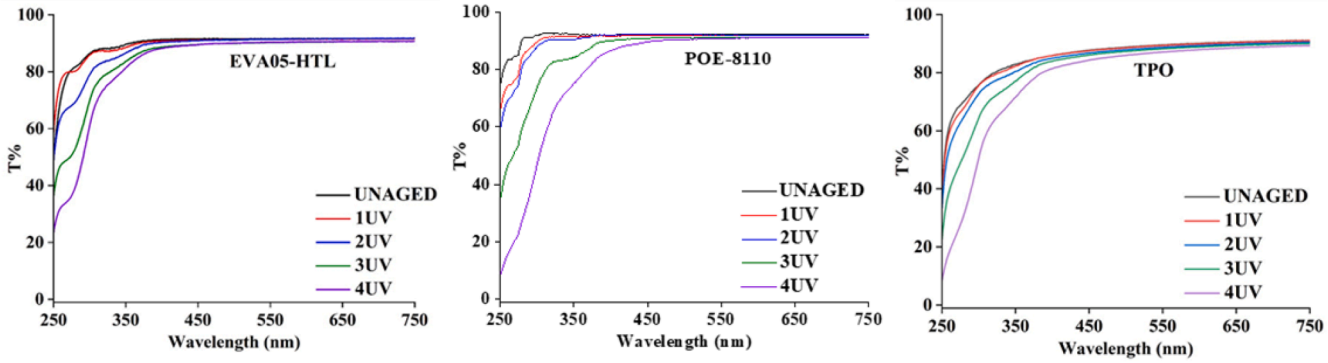



**Fig. 3.** UV–vis transmission spectra of encapsulants, before and after UV aging.

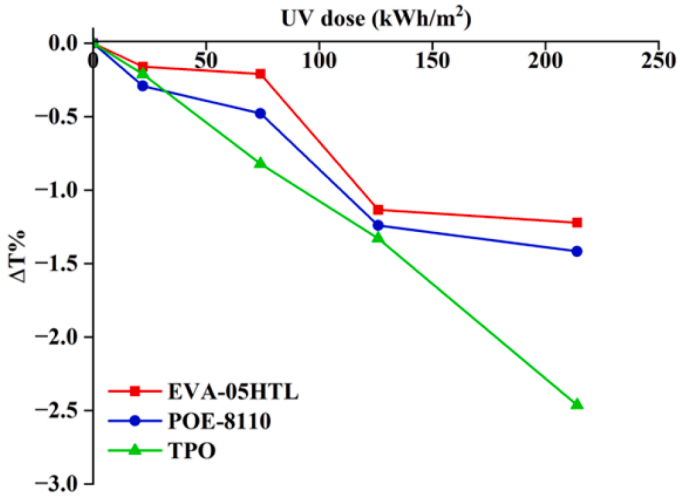



**Fig. 4.** Change in T% at 550 nm vs. UV dose for different encapsulants.

**Table 3**
Yellowing Index measurements for each encapsulant film, before and after UV aging.

| Sample | UV dose (kWh/m$^2$) | YI (average value) | Standard deviation | RSD % | ΔYI |
|---|---|---|---|---|---|
| EVA-05HTL | 0 | 1.77 | 0.06 | 3.15 | 0 |
| | 22 | 1.99 | 0.06 | 2.85 | 0.22 |
| | 74 | 2.69 | 0.12 | 4.46 | 0.92 |
| | 126 | 3.53 | 0.01 | 0.16 | 1.77 |
| | 214 | 3.84 | 0.08 | 2.18 | 2.07 |
| POE-8110 | 0 | 2.28 | 0.03 | 1.16 | 0 |
| | 22 | 2.41 | 0.04 | 1.50 | 0.18 |
| | 74 | 2.94 | 0.12 | 3.92 | 0.66 |
| | 126 | 3.38 | 0.16 | 4.60 | 1.1 |
| | 214 | 5.56 | 0.12 | 2.13 | 3.28 |
| TPO | 0 | 3.93 | 0.04 | 1.06 | 0 |
| | 22 | 4.21 | 0.13 | 2.97 | 0.29 |
| | 74 | 4.24 | 0.04 | 0.83 | 0.31 |
| | 126 | 4.69 | 0.10 | 2.18 | 0.77 |
| | 214 | 4.84 | 0.22 | 4.60 | 0.91 |

The shoulders present at around 265 nm, especially evident for EVA and POE, are associated to presence of small amounts of these additives, while those present at higher wavelengths (~310 nm), are associated to UV absorbers.

The samples also show a weak reflectance. TPO shows the major reflectance variation with wavelength, it reaches a maximum of 22 % at 263 nm and then decreases progressively to 9 % at 550 nm. Instead, the reflectance of EVA-05HTL and POE-8110 is about 8 % in the visible range and increases slightly in the UV range. The weak reflection peak of TPO in the UV region, is probably due to a presence of small amount of a UV blocking or absorbing agent, in its formulation.

The high transparency encapsulants, developed in the recently to gain in the power output of the PV module, have a still uncertain long-time durability. The reduced or avoided use of an appropriate UV stabilizers in their formulation certainly compromises their long-term durability and causes faster discoloration over time [29,30].

In order to study the effects of UV aging, all samples have been exposed to four UV doses: 22, 74, 126 and 214 kWh/m$^2$, indicated respectively with 1, 2, 3 and 4 UV, in a climatic chamber. To evaluate the variation in the optical properties of the three films caused by accelerated aging, UV–vis spectroscopic analyses were repeated after each step of exposure to UV rays. Fig. 3 shows the optical performance change of EVA-05HTL, POE-8110 and TPO, first and after accelerated UV aging.

The transmittance values of the samples progressively decrease over the exposure at four UV doses.

Light transmission of a good encapsulant should be >90 % and so that its optical properties can be considered constant, the loss of light transmittance after 20 years of operation should be <5 %. Within the visible wavelength range from 400 to 750 nm, there is a light degradation in transmittance after the fourth step of accelerated UV aging test. However, due to the lack of UV absorber, the UV radiation passes through the polymers and this results in discoloration and significant reduction in transmittance in the UV region. Lower is the wavelength of the UV light passing through the encapsulant, higher is its harmful effect on the polymer chain. The challenge is to extend the life of the modules using a high transparency encapsulant, resistant to the UV radiation harmful effects. In this respect, EVA-05HTL seems to be more performing.

After the fourth aging step, the change in % transmittance, at 550 nm, is greater for TPO (Fig. 4).

Encapsulants having UV absorbers tend to undergo faster discoloration as compared to those without UV absorbers [31]. Due to the presence of small amounts of UV absorbers, TPO undergoes a more rapid reduction in transmittance. EVA-05HTL exhibits more stable optical properties.

Since, UV absorption causes the polymers yellowing, resulting in loss of encapsulation efficiency, in order to confirm the discoloration, the Yellowness Index (YI), commonly used as a metric of the UV degradation, was measured before and after UV aging. To identify and assess the materials degradation, repeated colour measurements were performed on the samples. Measurements were taken at five different locations on the sample surface to get an average value. YI was calculated based on the standard ASTM E313-00, 2001 [32].

For each sample, the YI change (YI) has been calculated as the difference between the average value measured after each step of

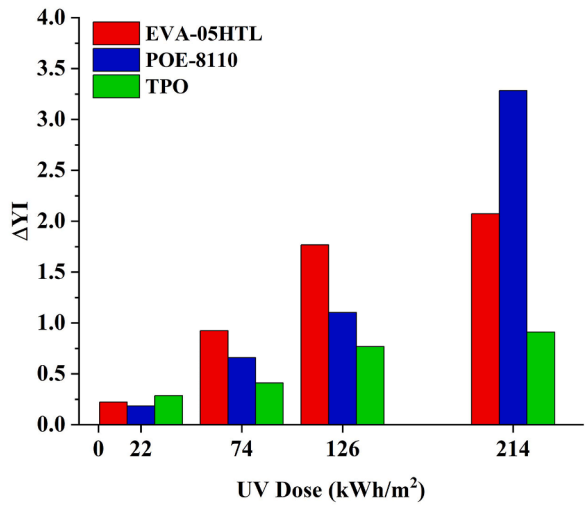



**Fig. 5.** Change in YI for the encapsulant films after UV aging test.

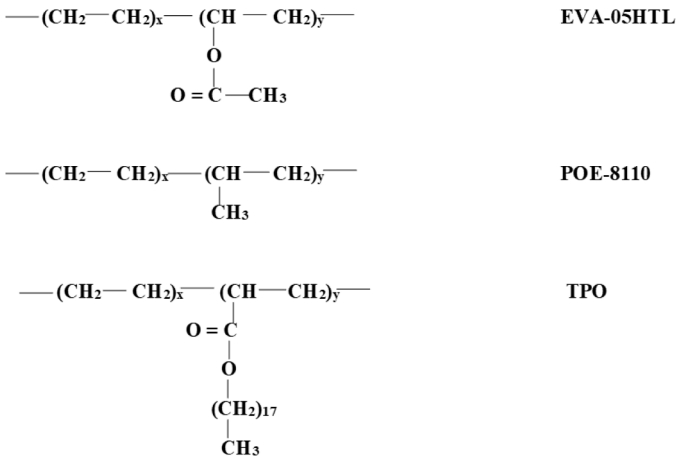



**Fig. 6.** Chemical structure of EVA-05HTL, POE-8110 and TPO.

exposition to UV dose and average value measured on the unaged sample.

The results of the colorimetric measurements carried out on the samples after each UV aging step, the mean YI values, standard deviation and the dispersion of the data with respect to the mean, are reported in Table 3. Since the RSD for all samples is less than 5 %, the YI measurements are indicative of a yellowing homogeneous distribution for each sample. Colour changes of the samples are shown in Fig. 5.

The change in YI is increased as the UV dose increases for all the encapsulant types. POE-8110 shows a major yellowing as compared to other materials, while TPO shows a minor increment in the change of YI value. EVA yellowing is favoured by the vinyl acetate loss and acetic acid production during the first step of molecule degradation [33]. The slower increment in TPO yellowing is probably due to its slightly higher reflectance as compared with the other samples, in the UV region, and to its lower fluorophore generation [22].

### 3.2. Chemical photo-degradation

Since the initial chemical structure of some PV encapsulants classes, such as POEs and TPOs, is often not clearly defined, it was determined and compared by FTIR analysis. EVAs, POEs and TPOs are made of a polyethylene backbone with different side groups [34]. FTIR analysis reveals that POE-8110 is an elastomeric copolymer of ethylene and propylene and TPO is a side-chain crystalline polymer: poly (ethylene-co-octadecyl acrylate) (Fig. 6).

POEs and TPOs can only be crosslinked using radical methods such as peroxides. Free radicals generated from the thermal decomposition of peroxides attack PE chains and crosslink the polymer [35]. TPO side-chain serves as structure-fixing network counterbalancing the cross-linked polymer network, subject to elastic deformation. It is found that lower cross-linking produces a higher degree of crystallinity and a higher stability of the polymer [36].

Fig. 7 shows the FTIR spectra of the three films analysed before and after UV aging. The peaks of PE backbone are at 720 $cm^{-1}$ ($CH_2$ skeleton rocking vibration), 1461 $cm^{-1}$ ($CH_2$ bending), 2850 $cm^{-1}$ ($CH_2$ symmetric stretching) and 2918 $cm^{-1}$ ($CH_2$ asymmetric stretching) [37,38]. EVA shows typical peaks of the vinyl acetate group at 1018 $cm^{-1}$ (C—O stretching), 1237 $cm^{-1}$ (C—O—C stretching), 1371 $cm^{-1}$ (C—H bending of methyl in VA group) and 1736 $cm^{-1}$ (C═O stretching) [39]. POE shows only a very weak signal around 1700 $cm^{-1}$, attributable to the presence of antioxidant additives [40]. TPO shows a significant peak at 1736 $cm^{-1}$ (C═O) and vibrations at 1200 $cm^{-1}$ (C—H), 1170 $cm^{-1}$ (C—C) and 1020 $cm^{-1}$ (C—O—C), most likely caused by acrylate units in its copolymeric backbone [29,41].

The peak of PE between 750 $cm^{-1}$ and 690 $cm^{-1}$ undergoes only small changes during UV exposure. Hence, the encapsulant degradation is mainly measured from the signal change assigned to C═O vibrational stretching [42]. This C═O vibrational stretching comes from the vinyl acetate (VA) unit in EVA and from acrylate units in TPO or also from additives added in the encapsulants formulation. In Fig. 7, the decrease in the peaks intensity associated with the C═O group of the ester (1736 $cm^{-1}$) is evident both in the spectrum of EVA-05HTL and in that of TPO. No C═O absorption is observed in the unaged POE-8110 spectrum. After UV exposure, C═O bands appeared and increased with increasing UV exposure. In the spectra of aged POE-8110 we can also see the formation of double bonds (1640 $cm^{-1}$). Furthermore, for all three samples, there is an increase in the peaks associated with the formation of degradation products: carboxylic acids (1695–1705 $cm^{-1}$), ketones (1713–1721 $cm^{-1}$), esters (1736 $cm^{-1}$), aldehydes (1733$cm^{-1}$) and lactones (1780 $cm^{-1}$). While the absorption frequency of esters and lactones does not change compared to the theoretical value that of carboxylic acids and ketones appears shifted to lower wavelength, for all samples. The absorption peak between 1695–1705 $cm^{-1}$, is probably due to the formation of γ-ketoacids, which have a lower absorption frequency than the associated carboxylic acids [43,44]. Moreover, the characteristic absorption peak of ketones, observed between 1713–1721 $cm^{-1}$, appears at lower frequencies in the case of EVA and POE, and slightly higher in the case of TPO. However, while the spectra of POE-8110 clearly show the new carbonyl functions formed during oxidation, the spectra of EVA-05HTL and TPO also include the initial carbonyl functions.

Therefore, to compare the photooxidation of the three films, a semi-quantitative analysis was performed only on the new formed carbonyl functions, specifically on carboxylic acids and ketones. The amount of the new carboxylic and ketone functions was calculated from the difference spectra in the spectrum region between 1800 and 1680 $cm^{-1}$, after baseline subtraction. The peaks area of the new functional groups was calculated by integrating and normalized with respect to the peak area of the methylene C—H symmetric stretching at 2850 $cm^{-1}$ [45]. In order to calculate the areas of the overlapping peaks , the deconvolution of the composite band profile was carried out by using Origin Pro Software [46]. The Carbonyl Index (CI) was calculated by Eq. (1):

$$\text{CarbonylIndex} = A_x/A_{2850} \quad (1)$$

where $A_{2850}$ is the peak area associated to the C—H stretching vibration of the methylene and $A_x$ is the area of the peak associated to the C═O stretching vibration of carboxylic acid and ketone. Peaks assignment was obtained by derivative analysis of the experimental curves and for the curve-fitting was used Gaussian function. All convergence solutions

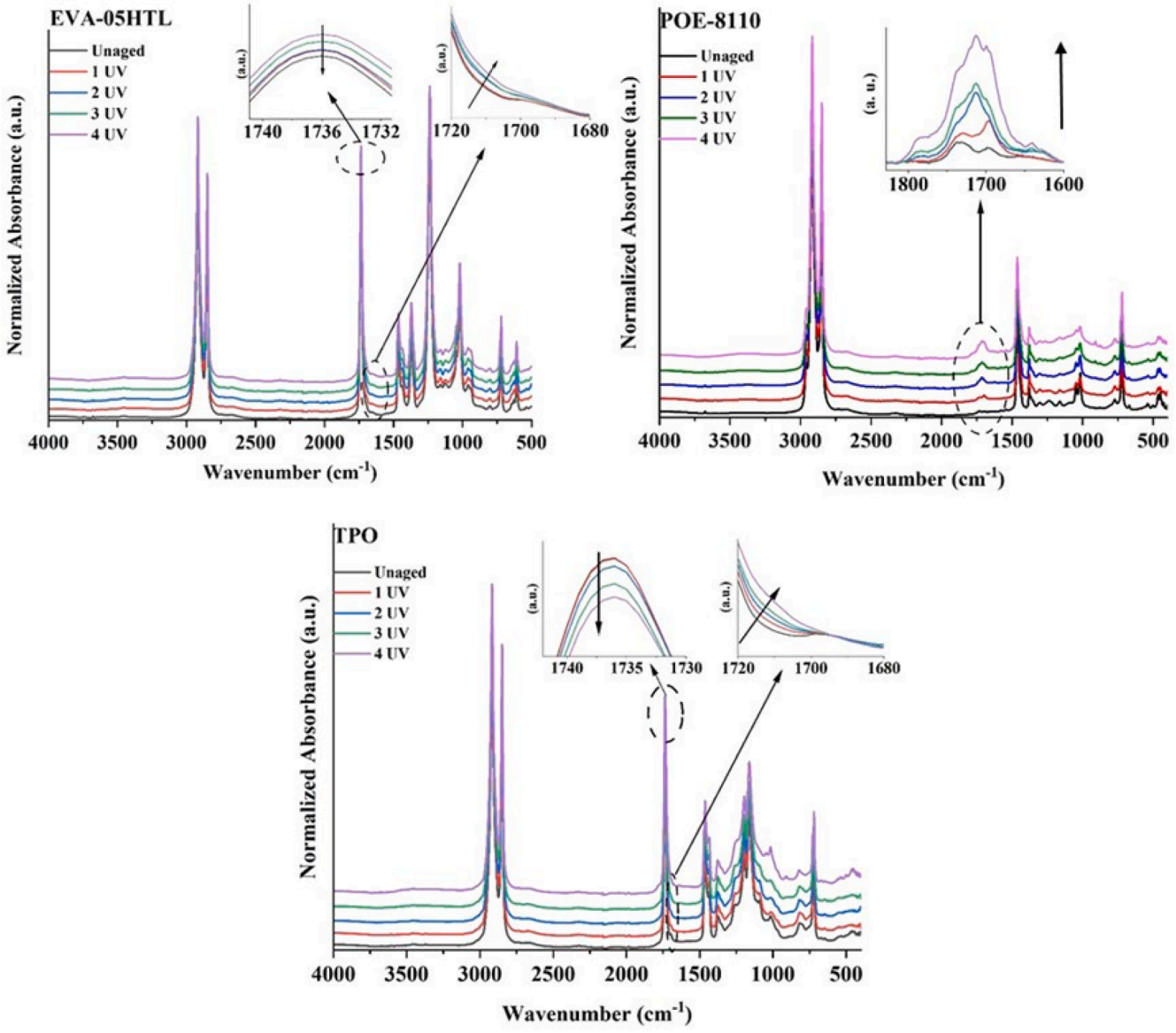



**Fig. 7.** ATR-FTIR spectra of EVA-05HTL, POE-8110 and TPO before and after UV aging.

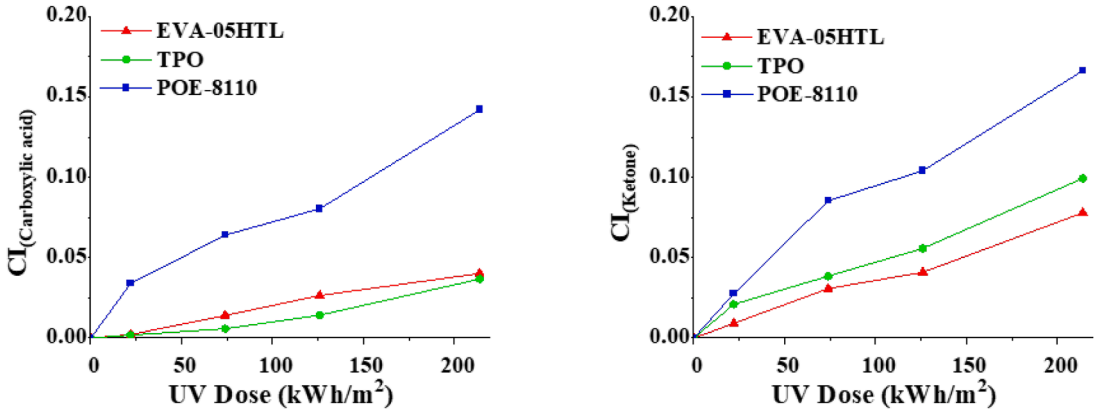



**Fig. 8.** Carbonyl index vs. UV dose for the three encapsulant films, referred to the variations of the C═O functional group in carboxylic acid and ketone.

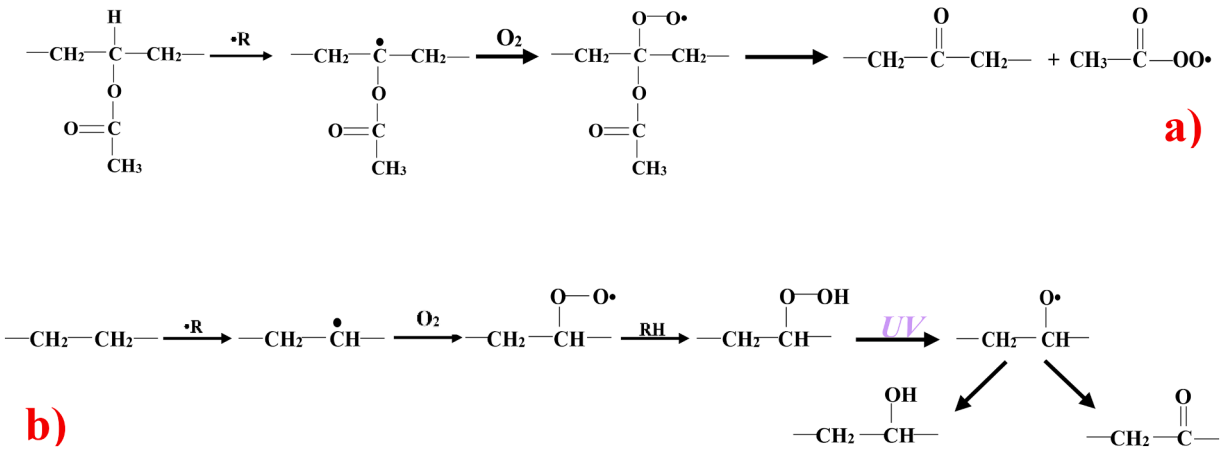



**Fig. 9.** Simplified scheme of photo-oxidation mechanism of EVA [48]. a) Branching chain and b) main chain.

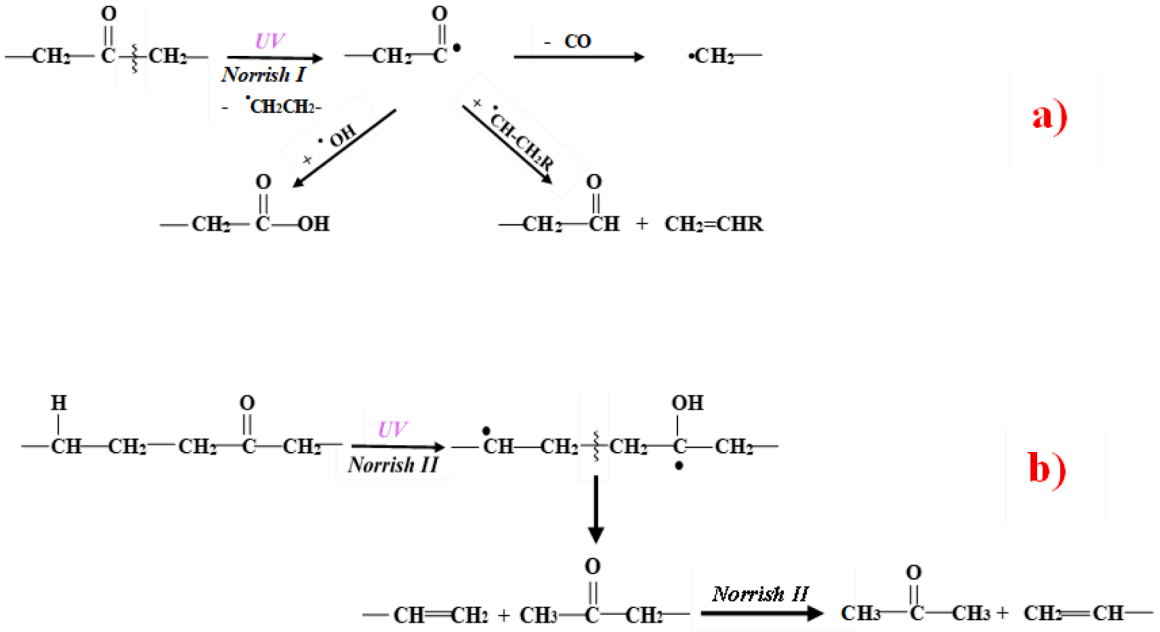



**Fig. 10.** Simplified scheme of Norrish reactions [50,52].

of the fit analyse have $R^2$ factor ≥0.995. The peaks of esters and aldehydes, at 1736 $cm^{-1}$ and 1733 $cm^{-1}$ respectively, are closely overlapped and cannot be resolved by deconvolution analysis.

The CIs of the three films, referred to carboxylic acids and ketones, calculated as a function of UV irradiation, are shown in Fig. 8. The increase in CI with increasing UV irradiation indicates that these oxidation products are formed in all films and the ketones are more abundant then carboxylic acids after aging. The CIs trend reveals that the least chemically stable encapsulant is POE-8110, while EVA-05HTL and TPO have comparable stability.

### 3.3. Photo-oxidation mechanism

UV radiation and temperature are the main sources of encapsulant degradation since have sufficient energy to exceed the dissociation energy of covalent bonds in the main chain of the polymer and promote its yellowing through the production of chromophores [47]. The breaking of the chemical bonds in the main chain triggers unwanted reactions that lead to the formation of radical species and small organic molecules [48].

The photo-oxidation of the encapsulant films is a radical chain process that takes place in 4 steps: initiation, propagation, branching and termination. Several functional groups such as hydroperoxides, esters, ketones and unsaturated sites are sensitive to photolytic attack. They can absorb UV radiation and even in the absence of oxygen, can undergo radical scission. The radicals can react following different pathways: abstraction of a hydrogen atom bonded to a carbon of the main chain, addition to an unsaturated group with crosslinking reaction, or addition to oxygen. During the initiation step, primary alkyl radicals are formed which have a short lifetime. Then, by hydrogen abstraction from the secondary or most favourable tertiary carbon atoms, more stable radicals are formed [49]. The primary photo-products that are formed are the hydroperoxides, which can decompose by the scission of the weak O—O bond, giving an alkoxy radical (•OR) and a hydroxyl radical (•OH). The •OR radical can react by several routes: β-scission with cleavage of the main chain to form aldehydes, abstraction of hydrogen without cleavage of the chain to form hydroxyls, reaction between the pair of the radicals formed, •OR and •OH, to produce ketones.

The main degradation pathway of EVA is represented in Fig. 9.

The interaction of ketones with UV-radiation can result in Norrish I and Norrish II reactions (Fig. 10). Norrish I reaction results in one acyl

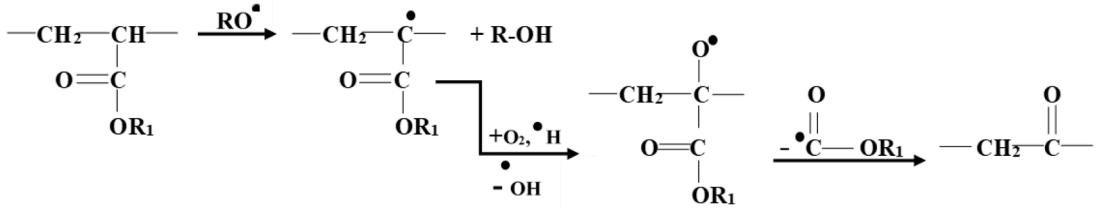


**Fig. 11.** Simplified mechanism of photo-oxidative degradation of acrylic polymers. General scheme proposed for the ketones formation initiated by free radicals.

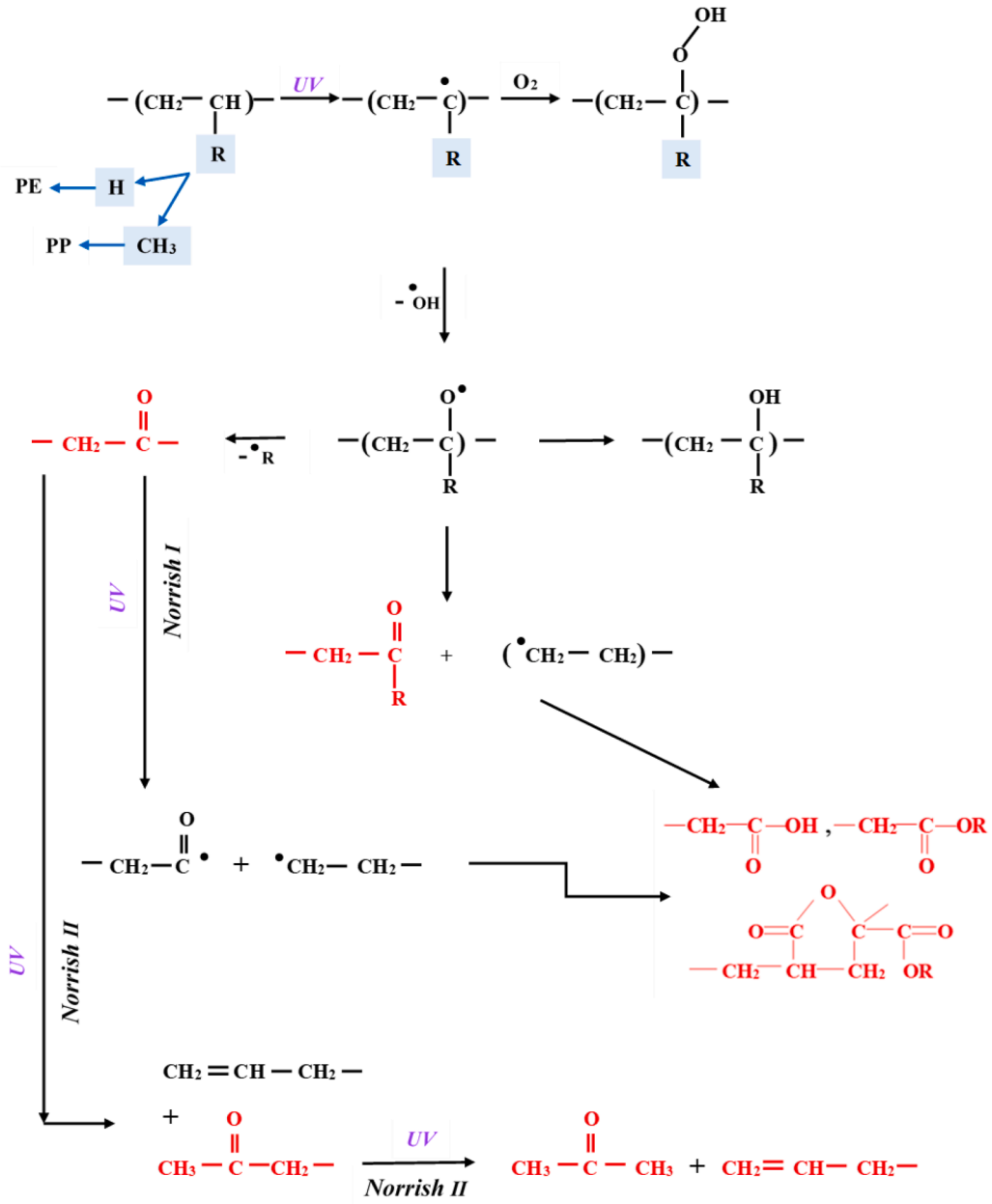


**Fig. 12.** Simplified mechanism proposed for the photo-oxidative degradation of POE.

and one alkyl radical. The acyl radical can recombine with a hydroxyl radical forming carboxylic acid or can release carbon monoxide forming another alkyl radical, so reducing the CI, or again, if the alkyl radical has a β-hydrogen it can react to form an alkene and an aldehyde. The Norrish II reaction causes the formation of a diradical by transposition of a γ-hydrogen onto the carbonyl oxygen and subsequently the β-scission of the polymer chain, with formation of a chain-end ketone and a polymer fragment with a vinyl end-group [50]. The chain-end ketone, in turn, also reacts by a Norrish II reaction forming a vinyl unsaturation and acetone [51].

The oxidative degradation of TPO probably initiates through reaction of oxygen molecules with the radicals formed by abstraction of the tertiary hydrogen atoms of the structural units. Subsequently, β-scission and formation of ketones occur according to scheme in Fig. 11 [53].

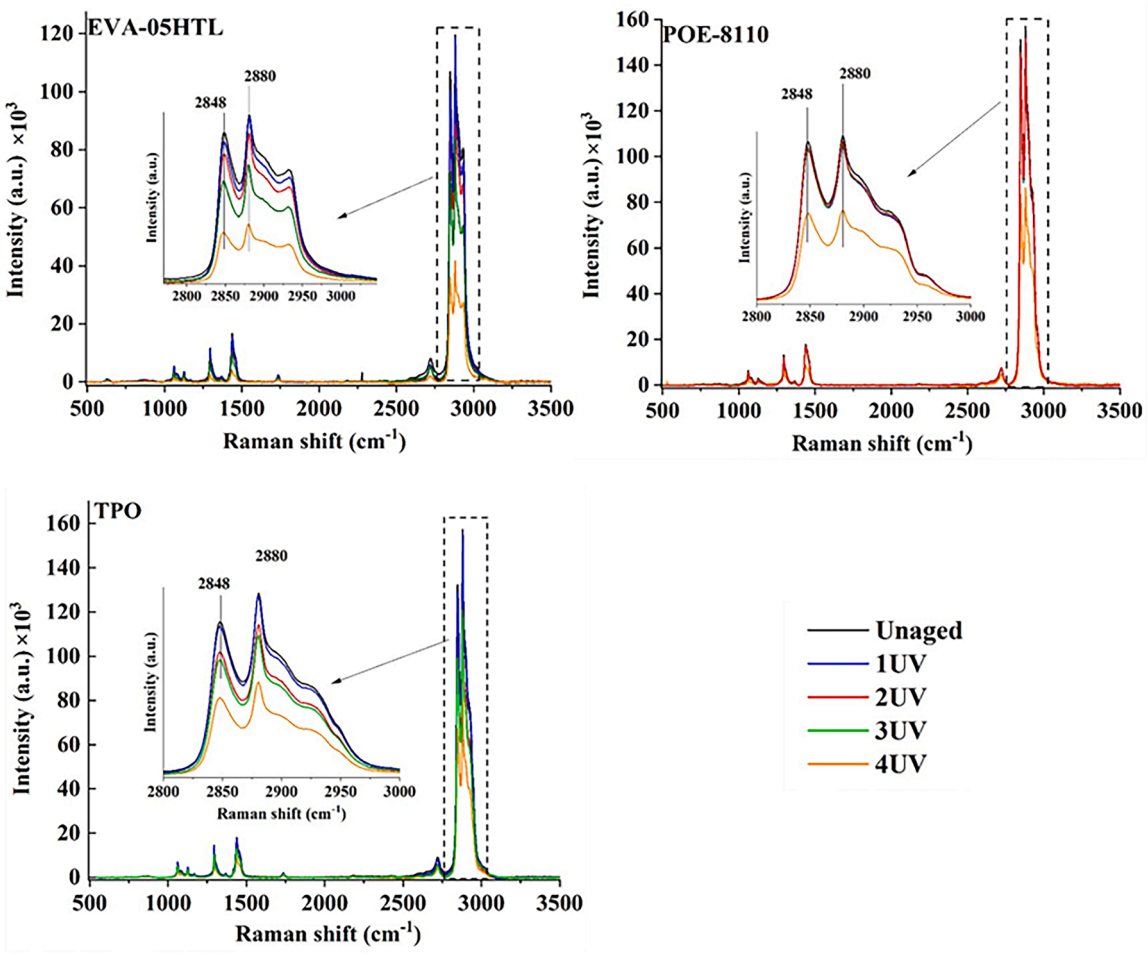



**Fig. 13.** Raman spectra of unaged and UV aged EVA-05HTL, POE-8110 and TPO films.

**Table 4**
Peaks and corresponding vibrational groups in Raman spectra in selected materials [19,59,60].

| Band characteristic | Assignment | Wavenumber ($cm^{-1}$) |
|---|---|---|
| O—C═O | deformation | 629 |
| C—C | asymmetric stretching of $CH_2$ | 1062 |
| C—C | symmetric stretching of $CH_2$ | 1126 |
| $CH_2$ | twisting | 1295 |
| $CH_2$ | wagging | 1416 |
| $CH_2$ | bending | 1438 |
| C═C | stretching | 1638 |
| C═O | stretching | 1736 |
| C—H | stretching | 2722 |
| $CH_2$ | symmetric stretching | 2848 |
| $CH_2$ | Fermi resonance | 2857 |
| $CH_2$ | asymmetric stretching | 2880–2890 |
| C—H | symmetric stretching | 2880–2890 |
| $CH_2$ | Fermi resonance | 2900 |
| $CH_3$ | symmetric stretching | 2880 |
| $CH_3$ | Fermi resonance | 2932 |
| $CH_3$ | asymmetric stretching | 2950 |
| $CH_3$ | asymmetric stretching | 2965 |

*Notation*: Fermi resonance between stretching modes and bending overtones.

Unsaturated sites in POE-8110 polymer are sensitive to photolytic attacks and to the thermo-oxidation. The presence of oxygen reduces the polymeric chain stability against photolytic attacks [50]. In Fig. 12 a simplified mechanism of POE photo-oxidation is reported. Photo-oxidation and thermo-oxidation produce almost the same oxidation products, apart from unsaturations that form only by photochemical processes. In both types of oxidations, the same carbonyl products are formed, but Norrish reactions that occur in photo-oxidation are responsible for the different relative concentrations. For example, ketones disappear to produce new unsaturations in photo-oxidation, while accumulate in thermo-oxidation [51,54].

Ketones photochemical degradation can take place according to Norrish type I or type II reactions. By Norrish II processes, vinyl-type unsaturations form and a chain-end ketone produces, which also reacts by a Norrish II reaction to form a vinyl unsaturation and acetone. By Norrish I reactions, through various reactions involving aldehydes and ketones radicals, form carboxylic acids, esters and lactones are produced [55].

All these degradation products, formed during exposure to UV radiation, are responsible for discoloration, delamination, and moisture permeability in the encapsulants and in particular, in the case of EVA acetic acid has an autocatalytic effect on yellowing. Generally, to enhance the outdoor durability of the encapsulants, additives such as curing agents which give a more cross-linked structure, UV absorbers and photo-thermal antioxidants are conveniently added in their formulation [28].

### *3.4. Raman spectroscopy and degradation of the polymer molecular structure*

The encapsulants photochemical degradation also involves the main polymer chain and results in the formation of conjugated polyenes as well as α,β-unsaturated carbonyl groups [56]. In order to evaluate the extent of the main chain degradation, the discoloration in the materials

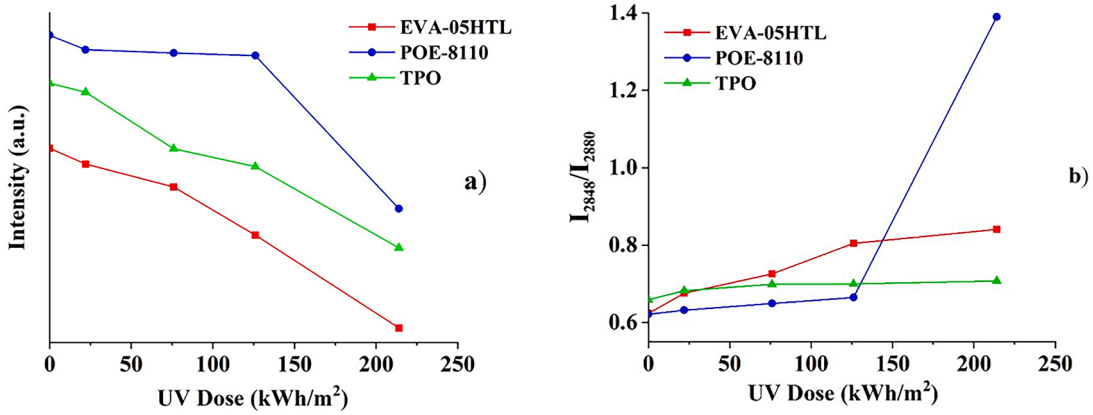



**Fig. 14.** a) Intensity difference of Raman peaks and fluorescence background for EVA-05HTL, POE-8110 and TPO. b) Intensity ratio of Raman peaks at 2848 ($CH_2$ units) and 2880 $cm^{-1}$ ($CH_3$ units) vs. UV dose, in EVA-05HTL, POE-8110 and TPO.

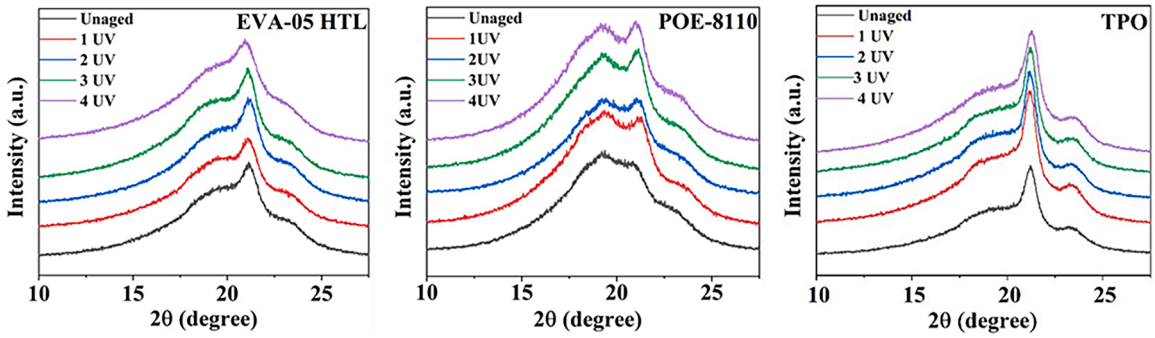



**Fig. 15.** X-ray diffraction of EVA-05HTL, POE-8110 end TPO sample before and after UV aging.

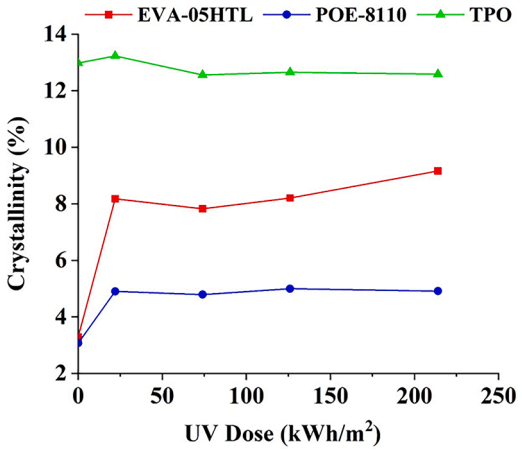



**Fig. 16.** Change in crystallinity of EVA-05HTL, POE-8110 and TPO during UV aging.

during UV aging, or to highlight the formation of chromophores groups that show fluorescence, Raman spectra were acquired and analysed before and after each exposure to UV radiation [57]. Due to the large dipole moment of the carbonyl groups and the consequent low sensitivity of the Raman signal towards them, identifying the degradation products such as acid, aldehyde, ketone is difficult because it is not possible to differentiate them from ester based on C═O stretching vibrations [58]. Then analysis of the Raman spectrum region, typical of these products, is generally not taken into account for evaluated the encapsulant degradation [42]. Instead, in order to study films degradation, the typical region of the aliphatic C—H band stretching vibrations, between 2800 and 3000 $cm^{-1}$ of the Raman spectra was investigated as these peaks have a strong scattering intensity. Raman spectra of the three sample under examination, before and after the UV aging, are shown in Fig. 13.

The vibrations of the main functional groups in selected materials are listed in Table 4.

Raman spectra of the samples show the characteristic peaks of the main polyethylenic chain which include the strong signals of $CH_x$ vibrational stretching in the range 2800–3025 $cm^{-1}$ [61]. A clear distinction of the three types of encapsulants is possible by the presence/absence of the carbonyl band at 1736 $cm^{-1}$. The polar nature of EVA, due to the presence of the O—C═O group of the VA unit, promotes the degradation of this polymer. The Raman spectra of EVA-05HTL show the C═O vibrational stretching at 1736 $cm^{-1}$ and the O—C═O deformation at 629 $cm^{-1}$, both involved in the degradation mechanism of EVA through the loss of the VA unit [60]. After aging, EVA spectra show a decrease of the 629 $cm^{-1}$ peak, due to the loss of O—C═O group as acetic acid during the first step of polymer degradation. Also the peak at 1736 $cm^{-1}$ decreases with increasing the UV dose for UV aged EVA-05HTL, while for POE-8110 these peaks are not detectable. In the case of TPO, Raman spectra show only the C═O vibrational stretching at 1736 $cm^{-1}$ related to the acrylate group present in its structure, as confirmed by ATR-FT-IR results.

The peaks in the range 2800–3025 $cm^{-1}$ are of special interest for the information on the scission of the main polymer chain during the UV aging. As the UV dose increases, the general and progressive decrease of the principal polymer peaks in the zone of the $CH_x$ stretching, reflects changes not only in the side groups, but also in the backbone structure, for all the encapsulants. This suggests that the polymer degradation causes volatilisation of small molecules, but also formation of monomer

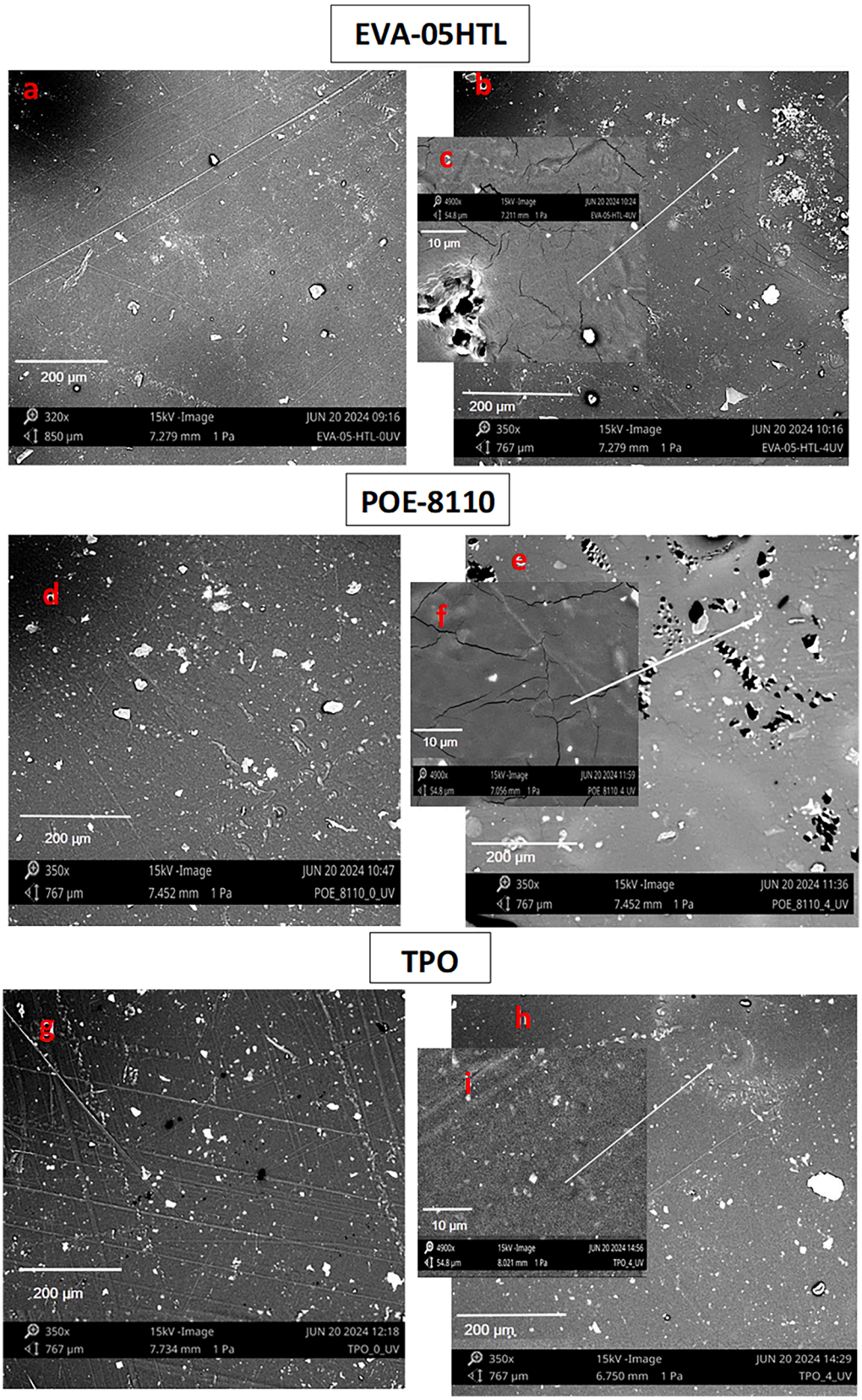



**Fig. 17.** SEM images of unaged EVA-05HTL (a) EVA-05HTL after 4UV (b, c), unaged POE-8110 (d) POE-8110 after 4UV (e, f), unaged TPO (g), TPO after 4UV (h, i).

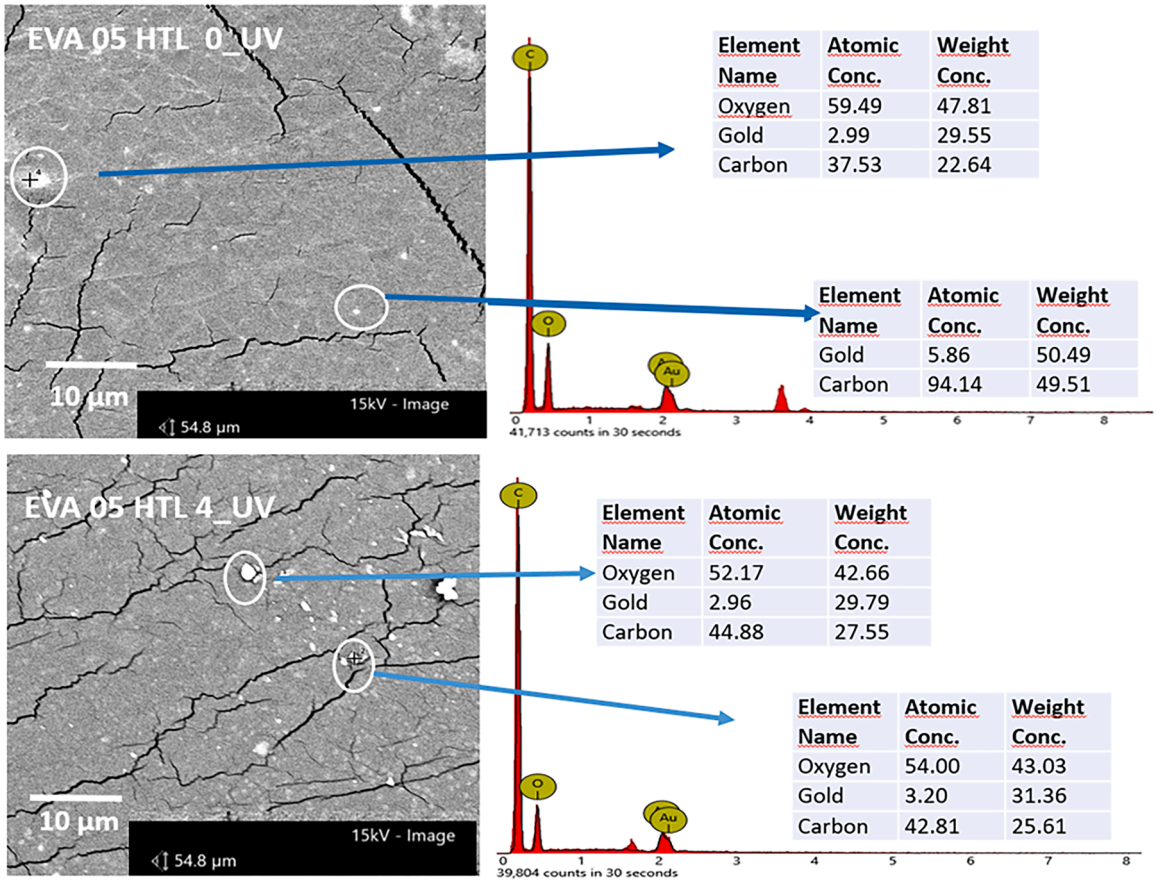



**Fig. 18.** EDX Analysis of EVA-05HTL, before and after UV aging.

molecules as a result of the chain scissions. The first signal of degradation of the encapsulants is the increase in intensity of the fluorescence background in the Raman spectra [62]. To highlight this increase in fluorescence, the difference between the intensity of the peak at 2848 $cm^{-1}$ and the background of the spectrum was calculated and shown in Fig. 14(a). For all encapsulants, the intensity at 1660 $cm^{-1}$ was considered as background. As the UV dose increases, the reduction in this difference indicates an increase in Raman fluorescence for all samples. In particular, for POE-8110, the intensity difference between the signals at 2848 and 1660 $cm^{-1}$ has a smaller initial decay and then after the third aging, a more significant drop. The increase in fluorescence between the beginning and the end of aging is of 66 %, 45 % and 49 % for EVA-05HTL, POE-8110 and TPO respectively.

During degradation, not only the absolute intensity of peaks related to the $CH_X$ vibration decrease, but also their relative intensities, due to production of volatile degradation products. Thus, the proportion of $CH_3$ groups compared to the $CH_2$ groups within the polymer backbone should decrease.

The peak at 2848 $cm^{-1}$ can be ascribed to $CH_2$ groups, whereas those at 2880 and 2932 $cm^{-1}$ to $CH_3$ groups. CH contributions are difficult to isolate due to the superposition with other modes forming the band at 2900 $cm^{-1}$ [59]. In order to isolate the individual contributions of $CH_3$, $CH_2$ and establish quantitative relationships between the signals intensities and their relative contributions, a curve-fitting analysis of Raman spectra was carried out. The deconvolution of the $CH_x$ stretching vibration region with 5 Lorentzian fits was carried out. The peaks at 2848, 2857, 2880, 2901 and 2932 $cm^{-1}$, typical of $CH_2$ and $CH_3$ vibrations, were considered. In particular, the symmetric stretching mode of the methylene group ($CH_2$) of the molecular main chain of polyethylene at 2848 $cm^{-1}$ and the asymmetric stretching mode of the methyl group (2880 $cm^{-1}$) were evaluated since they have high intensities and can be well detected. The intensity ratio of these two modes reveals a decrease of acetate groups in EVA-05HTL, of acrylate groups in TPO and of $CH_3$ in POE-8110, after aging [63]. As shown in Fig. 14(b), the chain scission leads to an increase in ratio $I_{2848}/I_{2880}$ [64]. POE-8110 is the encapsulant that shows the highest degradation, probably also because it doesn't contain UV absorbers or light stabilizing agents in its formulation.

Moreover, the intensity of the peak at 1416 $cm^{-1}$ ($CH_2$ wagging mode) is correlated to the crystallinity of the material's structure. Its intensity is stronger as well as higher the crystallinity of the material [65,66]. TPO spectra show a more defined peak at 1416 $cm^{-1}$ respect to a shoulder band present in the EVA-05HTL and POE-8110 spectra, indicating its higher crystallinity and after UV aging, this peak remains almost unchanged for the TPO.

### 3.5. Changes in crystallinity after UV aging

Crystalline properties of EVA-05HTL, POE-8110 and TPO samples and change in their crystallinity, during exposure to UV radiation, were determined by XRD analysis. The Fig.15 shows X-ray diffraction patterns of the three samples, analysed during UV exposure.

All samples present a marked amorphous phase covering the entire 2θ range. In fact, the X-ray patterns show a broad peak, highlighting a certain level of the organization in the internal structure of these encapsulants, but not the characteristic periodicity of a typical crystalline structure. They can be considered as complex semi-crystalline systems in which two polymers with a block structures having different densities coexistence [67]. All three samples have a crystalline phase at $2\theta = 21.5$.

The degree of crystallinity was calculated as the percentage of the scattered intensity of the crystalline phase over the sum of the scattered

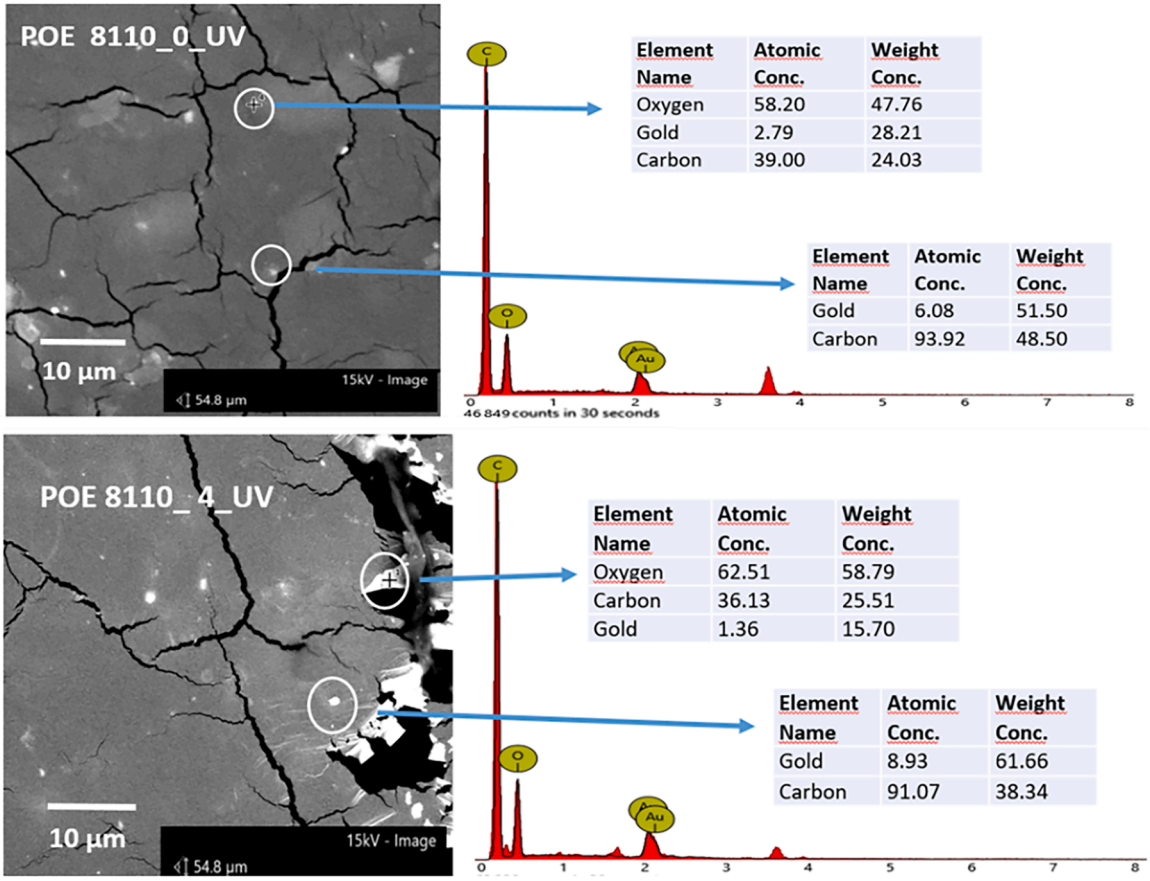



**Fig. 19.** EDX Analysis of POE-8110, before and after UV aging.

intensities of the crystalline and amorphous phases. The percentage crystallinity ($X_c$ %) was calculated using Eq. (2):

$$X_c(\%) = 100 \times [I_c / (I_c + I_a)] \quad (2)$$

where $I_c$ represents the sum of the intensities of crystalline sharp diffraction peaks, and $I_a$ represents the sum of the intensities of the amorphous diffuse scattering region. The determination of the crystalline phases of the polymers was carried out by deconvolution of the entire spectrum, using a Gauss peak for the crystalline phases and a Person peak for the amorphous ones. This choice was shown the best fitting between the experimental data and those of the model. Fig. 16 shows the change in crystallinity evaluated during UV aging.

EVA-05HTL and POE-8110 have a lower degree of crystallinity than TPO, due to their crosslinking. The crosslinking indeed prevents the segments with appropriate length from crystallizing and limits the arrangements of polymer chains in crystalline lattice, which results in smaller and imperfect crystals [68]. As well as reducing the degree of molecular organization by decreasing the degree of crystallinity, crosslinking also affects optical properties, by reducing the haze [7]. Unlike EVAs and POEs, peroxide-cured and crosslinked, TPOs do not crosslink chemically but form thermo-reversible physical crosslinks and exhibit higher crystallinity than other encapsulants [9]. Moreover, the long side groups in TPO give rigidity and structural stability to the molecule, and then a higher crystallinity. As the UV dose increases, the photochemical degradation leads to the loss of side groups. The segments of the chain that originally contain side groups are capable of rearranging themselves and forming crystalline structures. The decrease in the concentration of side groups leads to an increase in the crystallinity of the polymer. Aging induces the formation of shorter fragments, helps the molecules to organize themselves into crystalline phases and therefore increases the portions of this type compared to the amorphous portions.

In the case of EVA and POE, the increase in crystalline portions makes the molecules more ordered and these occupy less space. In this way, the dimensions of the material are reduced and breakage points or cracks are generated. As can be seen in Fig.18, EVA-05HTL and POE-8110 show an increase in crystallinity with increasing UV dose, while the crystallinity of the TPO does not show significant changes after UV aging and besides, its yellowing, due to chromophores formation that results in a decrease in transmittance, is opposed by the optical benefits from the slight reduction in crystallinity. EVA-05HTL is the film that undergoes the greatest change in crystallinity after exposure to UV radiation. The increase in crystallinity can cause embrittlement of the surface and thus can deteriorate the mechanical properties of the film [16]. This can affect the stability of the adhesion between encapsulant and other components of the PV module, resulting in the formation of cracks or delamination and also reduction of the protection of the cells against mechanical and thermo-mechanical loads [63].

### 3.6. Scanning electron microscopy analysis

In semicrystalline polymers, the haze is influenced by both morphology and surface topography. Therefore, the surface topography of the three samples were analysed before and after UV aging by SEM analysis. In Fig. 17, the surface of all samples appears relatively smooth, indicating that their haze has little relationship with the surface and is mainly related to the internal crystallinity [69]. Moreover, this analysis provides information on the extent of degradation.

As shown in Fig. 17b, the degradation is not particularly evident in the EVA-05HTL, after 4 UV, only small fractures and surface inhomogeneities appear. Compared to the unaged film (Fig. 17a), there are not significant signs of deterioration. The inset in Fig. 17c) provides in detail the effect of UV rays on the polymer film showing an area with

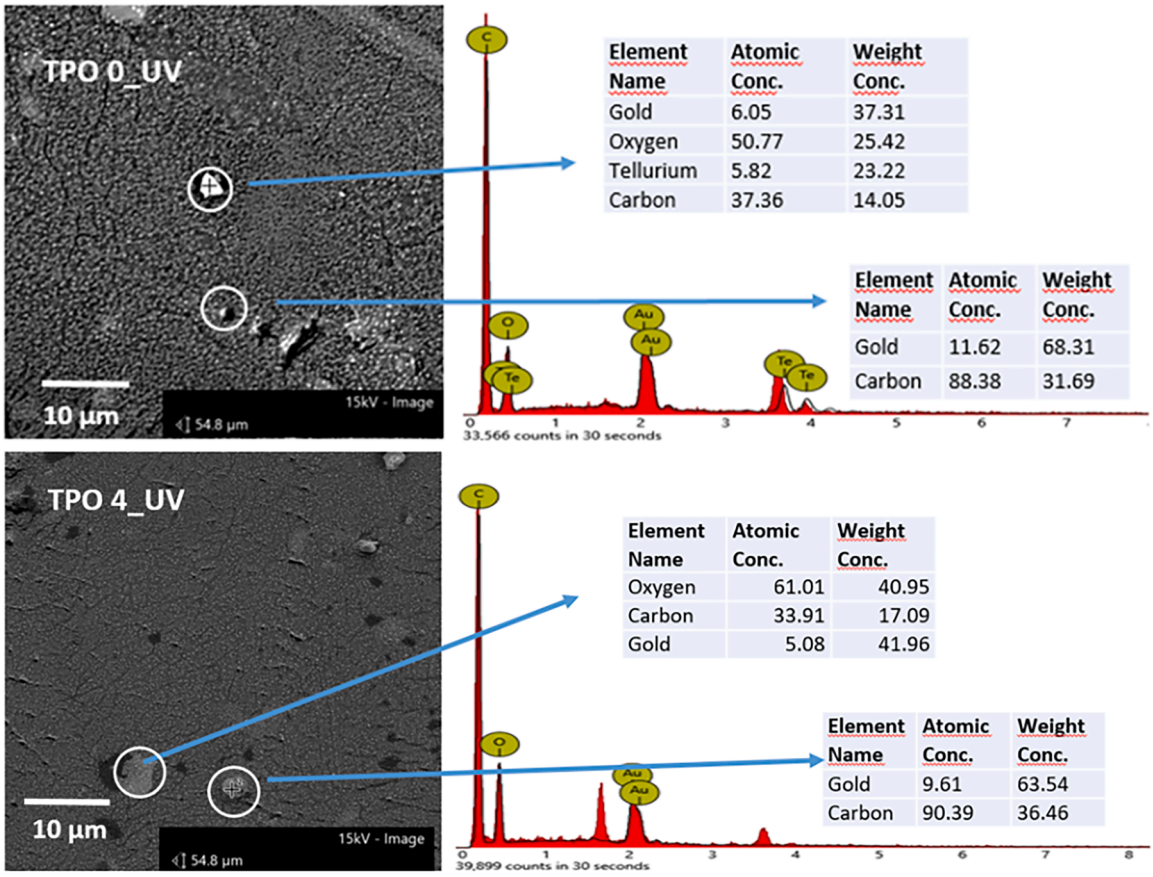



**Fig. 20.** EDX Analysis of TPO, before and after UV aging.

**Table 5**
Summary of the encapsulants properties after UV aging.

| Encapsulant | Δ (T%) at 550 nm | ΔYI | Chemical degradation | Crystallinity % | |
|---|---|---|---|---|---|
| | | | | Unaged | Δ($X_c$%) |
| EVA-05HTL | −1.22 | 2.07 | Low | 3.29 | 5.87 |
| POE-8110 | −1.42 | 3.28 | High | 3.07 | 1.84 |
| TPO | −2.46 | 0.91 | Low | 12.98 | −0.4 |

circular voids and small cracks.

Regarding POE-8110 (Fig. 17d), it can be observed that, superficial fractures occur and other signs of deep damage are present after 4 UV aging (Fig. 17e). The details are clearly visible in the inserted image (Fig. 17f). The presence of these superficial fractures indicates that, after aging, the film has undergone deep degradation and its surface structure has not remained intact.

The TPO films, both unaged (Fig. 17g) and after 4 UV (Fig. 17h, i), appear very similar to each other. Specifically, the TPO after 4 UV does not show any evident signs of damage. This observation suggests that UV exposure has not significantly affected the surface structure of the TPO film, keeping its initial characteristics unchanged.

A detailed analysis of the sample composition was carried out by using an EDX detector alongside the SEM. The agglomerates visible in the SEM images in Fig. 17 result from the thin gold coating on the samples surface, as confirmed by EDX analysis (Figs. 18–20). The metallization improves topographic contrast revealing surface fractures and pores. In the Figs. 18–20, the results of the EDX analysis are shown. They reveal that TPO has a better morphology, less invaded by agglomerates and without signs of deep fractures, after UV aging, compared to the other two samples, EVA and POE. Instead, the stress induced on the three encapsulants produces more significant effects on the POE-8110, as evidenced by the deep fractures in Fig. 19.

Furthermore, in the case of EVA, the oxygen/carbon ratio decreases

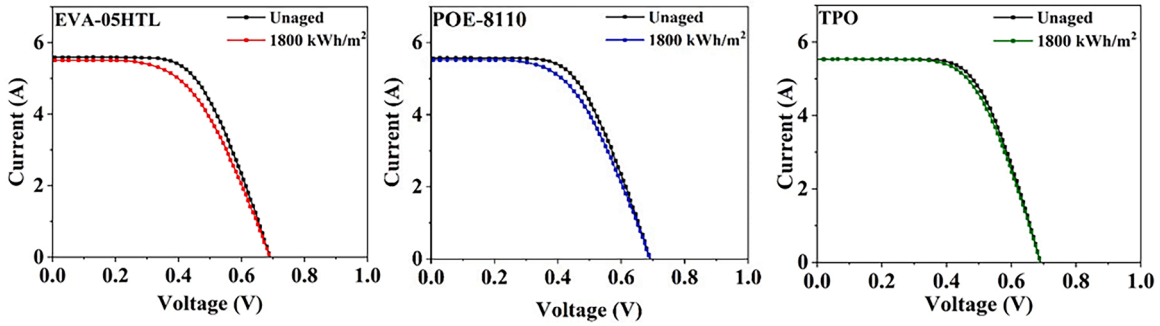



**Fig. 21.** I–V curves of mini-devices manufactured with a) EVA-05HTL, b) POE-8110 and c) TPO, before and after 1800 kWh/$m^2$ UV dose.

**Table 6**
Eff. (%), FF (%) and $P_{MPP}$ (W) values for mini-devices before (B) and after (A) UV aging.

| PV mini-device/ encapsulant | UV aging | Eff. (%) | ΔEff. (%) | FF (%) | ΔFF % | $P_{MPP}$ (W) | $\Delta P_{MPP}$ (%) |
|---|---|---|---|---|---|---|---|
| EVA-05HTL | B | 16.44 | | 58.56 | | 2.26 | |
| | A | 15.16 | −7.8 | 54.91 | −6.2 | 2.08 | −8.0 |
| POE-8110 | B | 16.45 | | 58.78 | | 2.27 | |
| | A | 15.46 | −6.0 | 55.32 | −5.9 | 2.13 | −6.2 |
| TPO | B | 17.42 | | 62.78 | | 2.39 | |
| | A | 16.48 | −5.4 | 59.42 | −5.4 | 2.27 | −5.0 |

after aging, probably indicating that the degradation undergone by the polymer is mainly due to deacetylation and only secondarily, to surface oxidation. Instead, in the case of POE and TPO, this ratio increases, indicating a degradation due only to the formation of oxidation products.

### 3.7. Results for encapsulant films

Table 5 provides an overview of the main findings for the examined encapsulants based on high transparency EVA, POE, TPO.

The elastomeric laminates exhibit low haze values both in the unaged state and in aged state, as shown by the T% slight change at 550 nm. Instead, TPO laminate has an already initially higher haze value and after UV aging, its T% decreases more.

The accelerated aging of the three films, due to exposure to UV radiation, determines the formation of oxidation products containing carbonyl groups, among which ketones are the most abundant. These degradation products are responsible for yellowing, delamination, bubble formation and therefore deterioration of the module. The trend of the CIs indicates that the least chemically stable encapsulant is POE-8110, while EVA-05HTL and TPO are more stable. The greater chemical degradation of POE-8110 is also confirmed by the RAMAN analysis which highlights a greater extent of degradation also affecting the main polymer chain. POE-8110 is also the encapsulant that shows the highest yellowing, while TPO shows only a low increment in the change of YI value.

The higher haze values of TPO were corroborated by higher degree of crystallinity. EVA-05HTL is the encapsulant film that undergoes the greatest change in crystallinity after exposure to UV radiation. EVA-05HTL and POE-8110 crystallinity increases with UV exposure, while for TPO does not show significant changes. The decrease in TPO transmittance, due to chromophores formation and to yellowing, is compensated by the optical benefits from the slight reduction in crystallinity.

### 3.8. PV mini-device testing

The effects of accelerated aging on the decay of the films properties are evident more quickly than those on the polymers enclosed in the mini-devices structure. In fact, the polymers encapsulated in the mini-devices have a smaller exposed surface than free polymers and therefore the harmful effects of UV radiation together with those of temperature and humidity, on the mini-devices are less dramatic than on free polymers, for the same absorbed UV dose.

To highlight the degradation in the electrical properties of the PV mini-devices made with the three different encapsulants, exposure to UV radiation was extended up to 1800 kWh/m$^2$ UV dose and at each aging step, the electrical parameters representing the performance of the cells were analyzed.

Different primary equivalent circuit parameters for different PV mini-devices, depend not only on the device design and in-house manufacturing process, but mainly on the materials used for the encapsulating. The analysis of these parameters allows to evaluate the

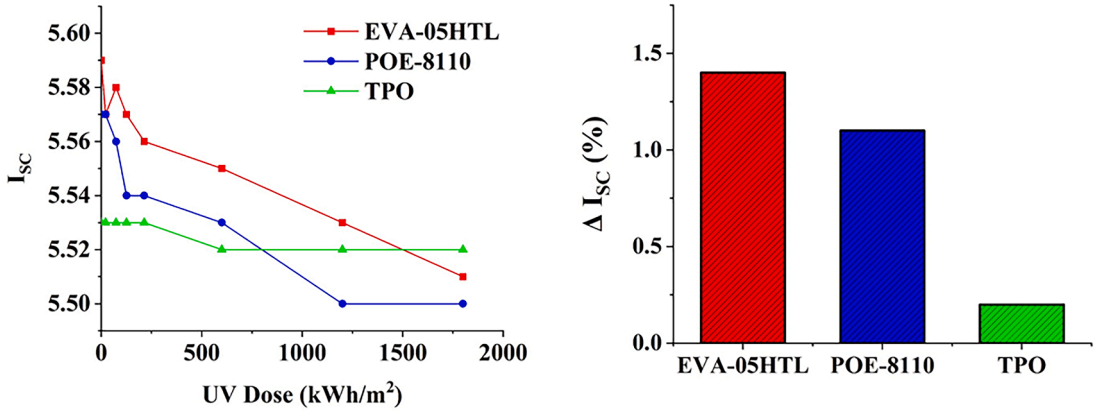



**Fig. 22.** $I_{SC}$ (a) and $I_{SC}$ variation % (b) at 1800 kWh/m$^2$ dose for three mini-devices before and after UV aging.

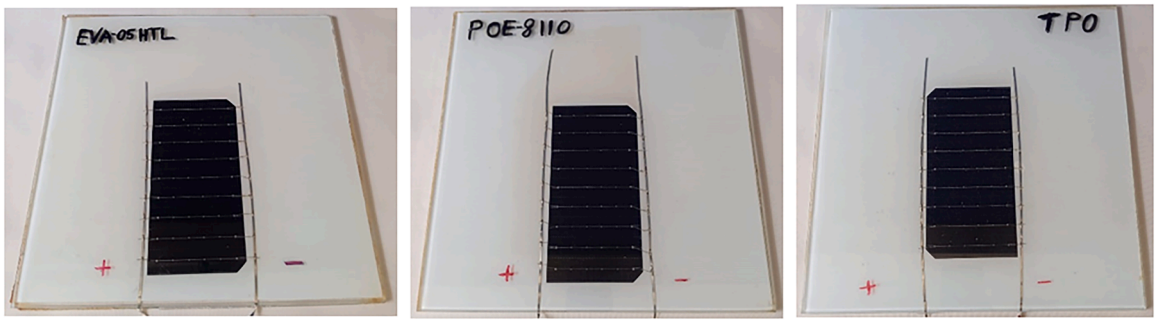



**Fig. 23.** Mini-devices manufactured with three different encapsulant films after UV aging.

link between stress induced by UV radiation, encapsulant materials properties and PV mini-devices electrical performance [70,71]. The solar cell equivalent circuit parameters were calculated from the measured I–V curves during module ageing. The changes in these parameters allow to evaluate whether UV exposure triggers different levels of degradation in devices made with different encapsulant films. The evolution of the I–V curves, during UV aging, for the three mini-devices, manufactured with EVA-05HTL, POE-8110 and TPO, is shown in Fig. 21.

All mini-devices show changes in the shape of the I–V curves and in the characteristic solar cell parameters, Eff., $P_{MPP}$ and FF, with a reduction of their values after 1800 kWh/m$^2$ UV dose, caused by degradation of the encapsulant materials induced by the applied stress conditions. Their electrical parameters and relative variations (%) at the end of the UV aging test, were reported in the Table 6.

Mini-devices made with EVA-05HTL and POE-8110 have a higher variation % of these three parameters than those made with TPO. The higher photo-degradation of these encapsulants results in a greater reduction in the performance of the mini-devices made with them. In verifying the performance and quality of a PV module and its constituents and at the same time efficiency losses and aging factors, FF is also an important parameter. In fact, it indicates the correct exploitation of the silicon wafer that constitutes the module; the higher it is, the higher the quality of the panel components and the lower the losses and the aging factors associated with them [72]. TPO undergoes the smallest FF loss after accelerated ageing.

The short-circuit current ($I_{SC}$), measured after each UV aging step as function of the UV dose, and its variation percentage after 1800 kWh/m$^2$ respect to $I_{SC}$ of the unaged mini-devices, are shown in Fig. 22.

All the mini-devices show a decrease of the $I_{SC}$ as the UV dose increases. Mini-devices made with EVA-05HTL and POE-8110 show a major decrement in the $I_{SC}$ values as compared to the mini-device made with TPO and EVA-05HTL shows a higher variation percentage in $I_{SC}$ (1.4 %), followed by POE-8110 (1.1 %). Mini-device made with TPO is the more stable with a variation of only 0.2 %

The images of the three mini-devices after UV light accelerated weathering tests are shown in Fig. 23.

Even with the naked eye, the mini-devices manufactured with EVA-05HTL and POE-8110 show a major discoloration respect to the mini-device made with TPO, caused by the chromophore formation after the photo-degradation of the encapsulant materials.

The results obtained for mini-devices may appear to be in contrast with the conclusions reached for polymer films as they are, but they can be explained by considering the different chemical compositions of the three classes of encapsulants subjected to aging. The presence of the acetate group in the EVA molecule, absent in POE and TPO, is the main cause of mini-device degradation. In fact, during aging, the deacetylation of EVA determines the development of acetic acid which, in the case of the film not enclosed in the mini-device structure, is free to move away from the polymer. Instead, in the case of EVA encapsulated in the mini-device, the developed acetic acid remains inside the structure, determining both the corrosion of the metals and the propagation of the degradation through chain reactions leading to the formation of by-products. Therefore, the mini-device made with EVA is the one that undergoes a greater drop in performance than the other two made with POE and TPO. Finally, the one made with TPO maintains its electrical properties slightly better than the one made with POE, at the same UV dose received, confirming the results obtained in the tests on the encapsulant films as they are.

## 4. Conclusion

This work discusses the reliability of PV devices fabricated with POs-based encapsulants, characterized by high UV transparency, used as an alternative to EVA, under realistic irradiation conditions. In particular, it studies the influence of stress factors such as UV radiation and temperature increase, on the performance of mini-devices made with EVA, POE and TPO, with high UV transparency, subjected to accelerated aging, pushed up to a UV dose of 1800 kWh/m$^2$. The electrical performances of the mini-devices made with POs-based films are compared with those of a mini-device made with EVA, pushing the UV aging test until evidence of degradation in the electrical performances of all the devices made with the different materials.

The amount of UV radiation from sunlight transmitted through each encapsulant and the temperature increase play a synergistic action in causing PV module degradation and have different influences on the structural integrity of the different polymers. During aging, all encapsulants undergo chemical degradation, evidenced by yellowing, polymer bond breaking, and the formation of oxidation products containing carbonyl groups. TPO is the most chemically stable polymer, as demonstrated by FTIR and RAMAN analysis and by the negligible change in its YI value. The CI trends and RAMAN analysis indicate that POE-8110 is instead the least chemically stable encapsulant. It is also the film that shows the highest yellowing.

After the accelerated aging test, the transmittance of all three encapsulants remains high. In fact, the UV spectroscopic analysis highlights for all of them only a slight variation in T% at 550 nm. Only TPO, which already has an initially lower T% value, undergoes a slightly more significant increase in the haze value, after aging. The slightly lower transmittance of TPO compared to other films is due to its higher degree of crystallinity. After exposure to UV radiation, TPO undergoes a negligible change in crystallinity, while the crystallinity of POE-8110 and especially that of EVA-05HTL increases. Therefore, the slight decrease in TPO transmittance is compensated by the optical benefits resulting from the slight reduction in crystallinity. The results obtained highlight that TPO is an interesting alternative to EVA.

As for the mini-devices, all of them show changes in the main characteristic solar cell parameters, Eff., PMPP and FF, after UV aging, but the most significant degradation was detected for the mini-device made with EVA-05HTL. This result is due to the presence of the acetate group in the EVA molecule, absent in POE and TPO, which leads to the production of acetic acid and determines both the corrosion of the metals and the propagation of degradation. Moreover, at the same UV dose received, the mini-devices made with POE and TPO maintain their performance better than the device made with EVA, not only because they do not produce acetic acid, but also because they are thermally more stable. Finally, the device made with TPO is chemically more stable and durable than the one made with POE, confirming the results obtained for the encapsulating films as they are. Further studies are underway to evaluate the moisture permeability in mini photovoltaic devices made with these new encapsulants and the influence of this other degradation factor on their reliability and durability.

## CRediT authorship contribution statement

**Valeria Fiandra:** Writing – review & editing, Writing – original draft, Supervision, Investigation, Data curation, Conceptualization. **Lucio Sannino:** Validation, Software, Methodology, Investigation, Data curation, Conceptualization. **Concetta Andreozzi:** Visualization, Validation, Software, Methodology, Formal analysis, Data curation. **Giovanni Flaminio:** Visualization, Validation, Software, Data curation. **Antonio Romano:** Software. **Gabriella Rametta:** Visualization, Validation, Formal analysis.

## Declaration of competing interest

The authors declare that they have no known competing financial interests or personal relationships that could have appeared to influence the work reported in this paper.

## Acknowledgements

Authors would like to acknowledge SATINAL spa, 3M Italia srl and

MG Lavorazioni Materie Plastiche Spa, for providing materials used in this work. The research work was supported by Italian Ministry of Environment and Energy Security in the framework of the Operating Agreement with ENEA for Research on the Electric System. This work also funded from the European Union's Horizon 2020 research and innovation programme under grant agreement no. 958223.

## Data availability

No data was used for the research described in the article.

## References

[1] G. Säckl, G.M. Wallner, J. Duchoslav, M. Tiefenthaler, D. Stifter, Advanced analysis of ethylene vinyl acetate copolymer materials for photovoltaic modules, Polym. Test. 132 (2024) 108381, https://doi.org/10.1016/j.polymertesting.2024.108381.
[2] N.Tz. Dintcheva, E. Morici, C. Colletti, Encapsulant materials and their adoption in photovoltaic modules: a brief review, Sustainability 15 (2023), https://doi.org/10.3390/su15129453.
[3] M. Landa-Pliquet, T. Béjat, M. Serasset, A. Descormes, E. Mofakhami, E. Voroshazi, Enhancing photovoltaic modules encapsulation: optimizing lamination processes for polyolefin elastomers (POE) through crosslinking behavior analysis, Sol. Energy Mater. Sol. Cells 267 (2024), https://doi.org/10.1016/j.solmat.2024.112725.
[4] P.M. Sommeling, J. Liu, J.M. Kroon, Corrosion effects in bifacial crystalline silicon PV modules; interactions between metallization and encapsulation, Sol. Energy Mater. Sol. Cells 256 (2023) 112321, https://doi.org/10.1016/j.solmat.2023.112321.
[5] M. Baiamonte, C. Colletti, A. Ragonesi, C. Gerardi, N.T. Dintcheva, Durability and performance of encapsulant films for bifacial heterojunction photovoltaic modules, Polymers (Basel) (2022) 14, https://doi.org/10.3390/polym14051052.
[6] B. Brune, I. Ortner, G.C. Eder, Y. Voronko, G. Oreski, K.A. Berger, K. Knöbl, L. Neumaier, M. Feichtner, Quantifying the influence of encapsulant and backsheet composition on PV-power and electrical degradation, Prog. Photovoltaics Res. Appl. 31 (2023) 716–728, https://doi.org/10.1002/pip.3679.
[7] S. Uličná, A. Sinha, D.C. Miller, B.M. Habersberger, L.T. Schelhas, M. Owen-Bellini, PV encapsulant formulations and stress test conditions influence dominant degradation mechanisms, Sol. Energy Mater. Sol. Cells 255 (2023), https://doi.org/10.1016/j.solmat.2023.112319.
[8] A.K. Schnatmann, F. Schoden, E. Schwenzfeier-Hellkamp, Sustainable PV module design—Review of state-of-the-art encapsulation methods, Sustainability 14 (2022), https://doi.org/10.3390/su14169971.
[9] G. Oreski, A. Omazic, G.C. Eder, Y. Voronko, L. Neumaier, W. Mühleisen, C. Hirschl, G. Ujvari, R. Ebner, M. Edler, Properties and degradation behaviour of polyolefin encapsulants for photovoltaic modules, Prog. Photovoltaics Res. Appl. 28 (2020) 1277–1288, https://doi.org/10.1002/pip.3323.
[10] S.K. Gaddam, R. Pothu, R. Boddula, Advanced polymer encapsulates for photovoltaic devices—A review, J. Mater. 7 (2021) 920–928, https://doi.org/10.1016/j.jmat.2021.04.004.
[11] C. Molto, J. Oh, F.I. Mahmood, M. Li, P. Hacke, F. Li, R. Smith, D. Colvin, M. Matam, C. DiRubio, G. Tamizhmani, H. Seigneur, Review of potential-induced degradation in bifacial photovoltaic modules, Energy Technol. 11 (2023) 1–30, https://doi.org/10.1002/ente.202200943.
[12] F. ibne Mahmood, G. TamizhMani, Impact of different backsheets and encapsulant types on potential induced degradation (PID) of silicon PV modules, Sol. Energy 252 (2023) 20–28, https://doi.org/10.1016/j.solener.2023.01.047.
[13] O. Arriaga Arruti, L. Gnocchi, Q. Jeangros, C. Ballif, A. Virtuani, Potential-induced degradation in bifacial silicon heterojunction solar modules: insights and mitigation strategies, Prog. Photovoltaics Res. Appl. 32 (2024) 304–316, https://doi.org/10.1002/pip.3765.
[14] M. Baiamonte, S. Therias, J.L. Gardette, C. Colletti, N.T. Dintcheva, Encapsulant polymer blend films for bifacial heterojunction photovoltaic modules: formulation, characterization and durability, Polym. Degrad. Stab. 193 (2021) 109716, https://doi.org/10.1016/j.polymdegradstab.2021.109716.
[15] D. Kim, H. Lim, S.H. Kim, K.N. Lee, J. You, D.Y. Ryu, J. Kim, Recent developments of polymer-based encapsulants and backsheets for stable and high-performance silicon photovoltaic modules: materials nanoarchitectonics and mechanisms, J. Mater. Chem. A 12 (2024) 7496, https://doi.org/10.1039/d3ta06130b.
[16] A. Fromm, A. Trondl, H. Strecker, M. Krappitz, D. Thissen, R. Kubler, 26th European photovoltaic solar energy conference and exhibition (26th EU PVSEC, in: European Commission (Ed.), 26th Eur. Photovolt. Sol. Energy Conf. Exhib, WIP-Renewable Energies, Hamburg, Germany, 2011, pp. 3121–3125. http://www.photovoltaic-conference.com.
[17] D.C. Miller, F. Alharbi, A. Andreas, J.G. Bokria, D.M. Burns, J. Bushong, X. Chen, D. Dietz, S. Fowler, X. Gu, A. Habte, C.C. Honeker, M.D. Kempe, H. Khonkar, M. Köhl, N.H. Phillips, J. Rivera, K.P. Scott, A. Singh, A.F. Zielnik, Degradation in photovoltaic encapsulation strength of attachment: results of the first PVQAT TG5 artificial weathering study, Prog. Photovoltaics Res. Appl. 28 (2020) 639–658, https://doi.org/10.1002/pip.3255.
[18] R. Witteck, B. Veith-Wolf, H. Schulte-Huxel, A. Morlier, M.R. Vogt, M. Köntges, R. Brendel, UV-induced degradation of PERC solar modules with UV-transparent encapsulation materials, Prog. Photovoltaics Res. Appl. 25 (2017) 409–416, https://doi.org/10.1002/pip.2861.
[19] B. Adothu, F.R. Costa, S. Mallick, UV resilient thermoplastic polyolefin encapsulant for photovoltaic module encapsulation, Polym. Degrad. Stab. 201 (2022), https://doi.org/10.1016/j.polymdegradstab.2022.109972.
[20] K.Y. Yang, J. Kim, H.K. Cho, T.J. Ha, Y.H. Kim, Environment-stable solar window modules encapsulated with UV-curable transparent resin, Sol. Energy 158 (2017) 528–532, https://doi.org/10.1016/j.solener.2017.10.002.
[21] J. Morse, M. Thuis, D. Holsapple, R. Willis, M.D. Kempe, D.C. Miller, Degradation in photovoltaic encapsulant transmittance: results of the second PVQAT TG5 artificial weathering study, Prog. Photovoltaics Res. Appl. 30 (7) (2022) 763–783, https://doi.org/10.1002/pip.3551.
[22] B. Adothu, P. Bhatt, S. Chattopadhyay, S. Zele, J. Oderkerk, H.P. Sagar, F. Reny, S. Mallick, Newly developed thermoplastic polyolefin encapsulant—A potential candidate for crystalline silicon photovoltaic modules encapsulation, Sol. Energy 194 (2019) 581–588, https://doi.org/10.1016/j.solener.2019.11.018.
[23] L. Liu, Y. Cheng, X. Zhang, Y. Shan, X. Zhang, W. Wang, D. Li, Graphene-based transparent conductive films with enhanced transmittance and conductivity by introducing antireflection nanostructure, Surf. Coat. Technol. 325 (2017) 611–616, https://doi.org/10.1016/j.surfcoat.2017.06.072.
[24] J. Eymard, R. Clerc, V. Duveiller, B. Commault, M. Hebert, Characterization of UV–vis–NIR optical constants of encapsulant for accurate determination of absorption and backscattering losses in photovoltaics modules, Sol. Energy Mater. Sol. Cells 240 (2022) 111717, https://doi.org/10.1016/j.solmat.2022.111717.
[25] B. Adothu, A.K. Singh, S. Kumar, S. Zele, S. Mallick, Effect of curing temperature on properties of ethylene vinyl acetate (EVA) used for crystalline silicon solar module encapsulation, in: EU PVSEC (Ed.), 36th Eur. Photovolt. Sol. Energy Conf. Exhib, Marseille, France, 2019, pp. 1200–1204, https://doi.org/10.4229/EUPVSEC20192019-4AV.2.31. https://www.researchgate.net/publication/339142348.
[26] D.C. Miller, M.T. Muller, M.D. Kempe, K. Araki, C.E. Kennedy, S.R. Kurtz, Durability of polymeric encapsulation materials forconcentrating photovoltaic systems, Prog. Photovoltaics Res. Appl. 21 (2013) 631–651, https://doi.org/10.1002/pip.1241.
[27] B. Adothu, P. Bhatt, S. Zele, J. Oderkerk, F. Reny, S. Mallick, Investigation of newly developed thermoplastic polyolefin encapsulant principle properties for the c-Si PV module application, Mater. Chem. Phys. 243 (2020) 122660, https://doi.org/10.1016/j.matchemphys.2020.122660.
[28] D.C. Miller, D.M. Burns, S. Fowler, L. Peter, C. Christian, N.H. Phillips, K.P. Scott, A.F. Zielnik, M. Köhl, M.D. Kempe, Degradation in photovoltaic encapsulant transmittance: results of the first PVQAT TG5 artificial weathering study, Prog. Photovoltaics Res. Appl. 27 (5) (2019) 391–409, https://doi.org/10.1002/pip.3103.
[29] R. Heidrich, C. Barretta, A. Mordvinkin, G. Pinter, G. Oreski, R. Gottschalg, UV lamp spectral effects on the aging behavior of encapsulants for photovoltaic modules, Sol. Energy Mater. Sol. Cells 266 (2024), https://doi.org/10.1016/j.solmat.2023.112674.
[30] S.I.N. Ayutthaya, J. Wootthikanokkhan, Investigation of the photodegradation behaviors of an ethylene/vinyl acetate copolymer solar cell encapsulant and effects of antioxidants on the photostability of the material, J. Appl. Polym. Sci. 107 (6) (2008) 3853–3863, https://doi.org/10.1002/app.27428.
[31] N. Pinochet, R. Couderc, S. Therias, Solar cell UV-induced degradation or module discolouration: between the devil and the deep yellow sea, Prog. Photovoltaics Res. Appl. 31 (2023) 1091–1100, https://doi.org/10.1002/pip.3725.
[32] F. Liu, L. Jiang, S. Yang, Ultra-violet degradation behavior of polymeric backsheets for photovoltaic modules, Sol. Energy 108 (2014) 88–100, https://doi.org/10.1016/j.solener.2014.06.027.
[33] B. Adothu, F. Reny, S. Mallick, Solar energy materials and solar cells damp heat resilient thermoplastic polyolefin encapsulant for photovoltaic module encapsulation, Sol. Energy Mater. Sol. Cells 224 (2021) 111024, https://doi.org/10.1016/j.solmat.2021.111024.
[34] Y. Bai, Y. Zhao, J. Li, H. Chen, A. Lambertz, Q. Qiu, C. Qian, J. Shi, W. Liu, T. Chen, J. Yu, K. Ding, J. Yu, Lower levelized cost of energy achievement of silicon heterojunction solar modules with low water vapor transmission rate encapsulants, Energy Technol. 11 (2023) 1–10, https://doi.org/10.1002/ente.202201466.
[35] R.I.N. Céspedes, J.F.H. Gámez, M.G.N. Velázquez, F.Á. Belmontes, R.E.D. De Leõn, O.S.R. Fernández, C.A.Á. Orta, E.H. Hernández, Thermoplastic elastomers based on high-density polyethylene, ethylene-propylene-diene terpolymer, and ground tire rubber dynamically vulcanized with dicumyl peroxide, J. Appl. Polym. Sci. 131 (2014) 1–8, https://doi.org/10.1002/app.39901.
[36] K. Liu, D.C. Miller, N. Bosco, R.H. Dauskardt, Determining the crosslinking and degradation reaction kinetics in photovoltaic encapsulants using accelerated aging, in: 52nd IEEE Photovolt. Spec. Conf. (PVSC52). NREL/CP-5K00-90303, Seattle, Washington, 2024. https://www.nrel.gov/docs/fy24osti/90303.pdf.
[37] A.P. Patel, A. Sinha, G. Tamizhmani, Field-aged glass/backsheet and glass/glass PV modules: encapsulant degradation comparison, in: IEEE J. Photovoltaics, 2156–3381, 2019 IEEE, Mesa, Arizona 85212 USA, 2020, pp. 607–615, https://doi.org/10.1109/JPHOTOV.2019.2958516.
[38] L. Spinella, S. Uličná, A. Sinha, D.B. Sulas-Kern, M. Owen-Bellini, S. Johnston, L. T. Schelhas, Chemical and mechanical interfacial degradation in bifacial glass/glass and glass/transparent backsheet photovoltaic modules, Prog. Photovoltaics Res. Appl. 30 (2022) 1423–1432, https://doi.org/10.1002/pip.3602.
[39] C. Barretta, G. Oreski, S. Feldbacher, K. Resch-Fauster, R. Pantani, Comparison of degradation behavior of newly developed encapsulation materials for photovoltaic applications under different artificial ageing tests, Polymers (Basel) 13 (2021) 271, https://doi.org/10.3390/polym13020271.
[40] M. Bredács, E. Kanatschnig, A. Frank, G. Oreski, G. Pinter, S. Gergely, Identifying active and degraded phenolic antioxidants in aged PE with IR-microscopy, Polym.

Degrad. Stab. 212 (2023), https://doi.org/10.1016/j.polymdegradstab.2023.110345.
[41] M. Tiefenthaler, G.M. Wallner, G. Säckl, F. Costa, Effect of UV ageing on debonding of double glass laminates based on different crosslinking and thermoplastic PV encapsulants, Sol. Energy Mater. Sol. Cells 273 (2024) 112965, https://doi.org/10.1016/j.solmat.2024.112965.
[42] C. Peike, T. Kaltenbach, K.A. Weiß, M. Koehl, Non-destructive degradation analysis of encapsulants in PV modules by Raman spectroscopy, Sol. Energy Mater. Sol. Cells 95 (2011) 1686–1693, https://doi.org/10.1016/j.solmat.2011.01.030.
[43] M. Salvalaggio, R. Bagatin, M. Fornaroli, S. Fanutti, S. Palmery, E. Battistel, Multi-component analysis of low-density polyethylene oxidative degradation, Polym. Degrad. Stab. 91 (2006) 2775–2785, https://doi.org/10.1016/j.polymdegradstab.2006.03.024.
[44] W. Yagoubi, A. Abdelha, M. Sebaa, S.F. Chabira, Identification of carbonyl species of weathered LDPE films by curve fitting and derivative analysis of IR spectra, Polymer Testing 44 (2015) 37–48, https://doi.org/10.1016/j.polymertesting.2015.03.008.
[45] B. Ottersböck, G. Oreski, G. Pinter, Comparison of different microclimate effects on the aging behavior of encapsulation materials used in photovoltaic modules, Polym. Degrad. Stab. 138 (2017) 182–191, https://doi.org/10.1016/j.polymdegradstab.2017.03.010.
[46] K. Yamada, S. Kumagai, T. Shiratori, T. Kameda, Y. Saito, A. Watanabe, C. Watanabe, N. Teramae, T. Yoshioka, Combined UV-irradiation and pyrolysis-GC/MS approach for evaluating the deterioration behavior of ethylene vinyl acetate, Polym. Degrad. Stab. 190 (2021) 109623, https://doi.org/10.1016/j.polymdegradstab.2021.109623.
[47] M.C.C. de Oliveira, A.S.A. Diniz Cardoso, M.M. Viana, V. de Freitas Cunha Lins, The causes and effects of degradation of encapsulant ethylene vinyl acetate copolymer (EVA) in crystalline silicon photovoltaic modules: a review, Renew. Sustain. Energy Rev. 81 (2018) 2299–2317, https://doi.org/10.1016/j.rser.2017.06.039.
[48] M. Gagliardi, P. Lenarda, M. Paggi, A reaction-diffusion formulation to simulate EVA polymer degradation in environmental and accelerated ageing conditions, Sol. Energy Mater. Sol. Cells. 164 (2017) 93–106, https://doi.org/10.1016/j.solmat.2017.02.014.
[49] J. Pilař, M. Slouf, D. Michalkova, I. Sloufova, T. Vackova, J. Dybal, Pro-oxidant activity of a-tocopherol during photooxidative degradation of polyolefins. ESRI and IR microspectroscopy studies, Polym. Degrad. Stab. 138 (2017) 55–71, https://doi.org/10.1016/j.polymdegradstab.2017.02.008.
[50] G. Grause, M.-F. Chien, C. Inoue, Changes during the weathering of polyolefins, Polym. Degrad. Stab. 181 (2020) 109364, https://doi.org/10.1016/j.polymdegradstab.2020.109364.
[51] M. Gardette, A. Perthue, J.L. Gardette, T. Janecska, E. Földes, B. Pukánszky, S. Therias, Photo- and thermal-oxidation of polyethylene: comparison of mechanisms and influence of unsaturation content, Polym. Degrad. Stab. 98 (2013) 2383–2390, https://doi.org/10.1016/j.polymdegradstab.2013.07.017.
[52] A. Parretta, M. Bombace, G. Graditi, R. Schioppo, Optical degradation of long-term, field-aged c-Si photovoltaic module, Sol. Energy Mater. Sol. Cells 86 (2005) 349–364, https://doi.org/10.1016/J.solmat.2004.08.006.
[53] O. Chiantore, L. Trossarelli, M. Lazzari, Photooxidative degradation of acrylic and methacrylic polymers, Polymer (Guildf) 41 (2000) 1657–1668, https://doi.org/10.1016/S0032-3861(99)00349-3.
[54] B. Hervé, G. Rapp, P.O. Bussiere, J.L. Gardette, S. Therias, Use of fluorescent probes in supporting functional group analysis resulting from polymer ageing, Polym. Degrad. Stab. 177 (2020), https://doi.org/10.1016/j.polymdegradstab.2020.109167.
[55] E. Mazeau, A. Duchamp, G. Pichon, B. Bouchut, J. Christmann, S. Therias, J. L. Gardette, Influence of chemical structural defects on the photostability of low-density polyethylene, Polym. Degrad. Stab. 228 (2024), https://doi.org/10.1016/j.polymdegradstab.2024.110921.
[56] A. Jentsch, K.J. Eichhorn, B. Voit, Influence of typical stabilizers on the aging behavior of EVA foils for photovoltaic applications during artificial UV-weathering, Polym. Test. 44 (2015) 242–247, https://doi.org/10.1016/j.polymertesting.2015.03.022.
[57] H. Han, H. Yan, X. Wang, K. Zhang, J. Huang, Y. Sun, J. Liu, P.J. Verlinden, P. Altermatt, Z. Liang, H. Shen, Analysis of the degradation of encapsulant materials used in photovoltaic modules exposed to different climates in China, Sol. Energy 194 (2019) 177–188, https://doi.org/10.1016/j.solener.2019.10.014.
[58] C.C. Lin, P.J. Krommenhoek, S.S. Watson, X. Gu, Depth profiling of degradation of multilayer photovoltaic backsheets after accelerated laboratory weathering: cross-sectional Raman imaging, Sol. Energy Mater. Sol. Cells 144 (2016) 289–299, https://doi.org/10.1016/j.solmat.2015.09.021.
[59] J.P. Tomba, L.I. Silva, M. García Genga, G. Barrera Galland, C.J. Perez, Characterizing chemical composition of polyolefin-based copolymers from spectral features in the C–H stretching region, J. Raman Spectrosc. 50 (2019) 576–586, https://doi.org/10.1002/jrs.5554.
[60] B.S. Chernev, C. Hirschl, G.C. Eder, Non-destructive determination of ethylene vinyl acetate cross-linking in photovoltaic (PV) modules by Raman spectroscopy, Appl. Spectrosc. 67 (2013) 1296–1301, https://doi.org/10.1366/13-07085.
[61] M. Bredács, C. Barretta, L.F. Castillon, A. Frank, G. Oreski, G. Pinter, S. Gergely, Prediction of polyethylene density from FTIR and Raman spectroscopy using multivariate data analysis, Polym. Test. 104 (2021), https://doi.org/10.1016/j.polymertesting.2021.107406.
[62] J. Correra-Puerta, P. Ferrada, P. Haberle, D. Diaz-Almeida, A. Sanz, O. Zubillaga, A. Marzo, C. Portillo, V. del Campo, Comparing the effects of ultraviolet radiation on four different encapsulants for photovoltaic applications in the Atacama Desert, Sol. Energy 228 (2021) 625–635, https://doi.org/10.1016/j.solener.2021.10.003.
[63] T. Meier, C. Peike, T. Kaltenbach, K.-A. WeißCaron, Changes of morphology and material properties of thin ethylene-vinyl acetate films under different aging conditions, in: 28th Eur. PV Sol. Energy Conf. Exhib., 28th European PV Solar Energy Conference and Exhibition, Paris, France, 2013. https://www.ise.fraunhofer.de/content/dam/ise/de/documents/publications/conference-paper/28-eupvsec-2013/meier.pdf.
[64] J. Zhang, F. Xu, X. Chen, C. Putson, S. Diaham, Q. Wang, Investigation of the potential-induced aging phenomenon of an insulating encapsulant for a photovoltaic module: from electrical to chemical properties, Appl. Energy Mater. 5 (2022) 5551–5560, https://doi.org/10.1021/acsaem.1c03521.
[65] A. Sinha, K. Hurst, S. Uličná, L.T. Schelhas, D.C. Miller, P. Hacke, Assessing UV-induced degradation in bifacial modules of different cell technologies, in: 2021 IEEE 48th Photovolt. Spec. Conf, Fort Lauderdale, FL, USA, 2021, pp. 0767–0770, https://doi.org/10.1109/PVSC43889.2021.9518728.
[66] S. Deng, Z. Zhang, C. Ju, J. Dong, Z. Xia, X. Yan, T. Xu, G. Xing, Research on hot spot risk for high-efficiency solar module, Energy Procedia 130 (2017) 77–86, https://doi.org/10.1016/j.egypro.2017.09.399.
[67] K. Agroui, G. Collins, Determination of thermal properties of crosslinked EVA encapsulant material in outdoor exposure by TSC and DSC methods, Renew. Energy 63 (2014) 741–746, https://doi.org/10.1016/j.renene.2013.10.013.
[68] K. Wang, Q. Deng, The thermal and mechanical properties of poly(ethylene-co-vinyl acetate) random copolymers (PEVA) and its covalently crosslinked analogues (cPEVA), Polymers (Basel) 11 (2019) 1055, https://doi.org/10.3390/polym11061055.
[69] A. Shamim, M. Noman, A.D. Khan, Reflection losses analysis from interspacing between the cells in a photovoltaic module using novel encapsulant materials and backsheets, Materials (Basel) 12 (2019), https://doi.org/10.3390/ma12132067.
[70] J. Zhu, M. Koehl, S. Hoffmann, K.A. Berger, S. Zamini, I. Bennett, E. Gerritsen, P. Malbranche, P. Pugliatti, A. Di Stefano, F. Aleo, D. Bertani, F. Paletta, F. Roca, G. Graditi, M. Pellegrino, O. Zubillaga, F.J.C. Iranzo, A. Pozza, T. Sample, R. Gottschalg, Changes of solar cell parameters during damp-heat exposure, Prog. Photovoltaics Res. Appl. 24 (2016) 1346–1358. 10.1002/pip.2793.
[71] S. Chattopadhyay, C. Solanki, K. Narasimhan, J. Vasi, S. Chattopadhyay, C. S. Solanki, A. Kottantharayil, K.L. Narasimhan, J. Vasi, S. Tatapudi, G. Tamizhmani, Quantification of PV module discoloration using visual image analysis, in: 2017 IEEE 44th Photovolt. Spec. Conf. (PVSC)- June 25–30, 2017, United States, Washington DC, 2017:, pp. 1850–1854, https://doi.org/10.1109/PVSC.2017.8366593.
[72] D.M. Atia, A.A. Hassan, H.T. El-Madany, A.Y. Eliwa, M.B. Zahran, Degradation and energy performance evaluation of mono-crystalline photovoltaic modules in Egypt, Cairo, Egypt, 2023. 10.1038/s41598-023-40168-8.